

Master's Thesis of Climate Studies

---

# **Dry Season Shallow Cumulus Clouds in the Amazon Rainforest**

---



WAGENINGEN UNIVERSITY  
METEOROLOGY AND AIR QUALITY

Author:

Xuemei Wang

Supervisor:

Prof. Jordi Vilà-Guerau de Arellano

Feb 28, 2018



## **MSc thesis Meteorology and Air Quality, Wageningen University**

Title: The influence of deforestation on shallow cumulus clouds in the Amazon rainforest

Date: Feb 28<sup>th</sup>, 2018

Author: Xuemei Wang

MSc Supervisor: Prof. Jordi Vilà-Guerau de Arellano

Assessment committee: Prof. Jordi Vilà-Guerau de Arellano  
Prof. Maarten Krol





## Abstract

The interactions between land and atmosphere regulate the formation of the shallow cumulus clouds through the thermals and moisture content. Several studies used the observations and models and showed that land properties altered by the deforestation effects in the Amazon rainforest had great influences on the shallow cumulus clouds. Large-eddy simulation (LES) has good resolutions in solving the turbulence that is related to the clouds formation, however, it is not used to thoroughly study the shallow cumulus clouds formation. Therefore, this study made use of LES, surface measurements and the radio soundings from the Amazon rainforest in a dry season month and investigated the effects of deforestation on the shallow cumulus clouds. In this study, the surface albedo, roughness length and leaf area index (LAI) are considered as important factors changed by deforestation. Therefore, we firstly validated the LES by the 30-day average of the observations which represented a typical dry-season day in the Amazon rainforest. Then we coupled a land surface model which activated the land-atmosphere interactions and set the surface properties as a grassland with the initial soil moisture index kept constant at 0.56. Lastly, we conducted several sensitivity experiments which changed the three deforestation related variables to the forest values. We found an overall reduction of cloud cover by more than 10% and a decline of liquid water path at  $10 \text{ g m}^{-2}$ . Furthermore, the shallow cumulus clouds were less unstable with deforestation and showed less probabilities for deeper convection.



# Contents

<b>Abstract</b>	<b>ii</b>
<b>List of Figures</b>	<b>v</b>
<b>List of Tables</b>	<b>v</b>
<b>1 Introduction</b>	<b>1</b>
<b>2 Methodology</b>	<b>4</b>
2.1 Datasets . . . . .	4
2.2 Experimental Design . . . . .	5
2.2.1 Initial LES model setup - offline . . . . .	6
2.2.2 The setup of Land Surface Model - online grassland control . . . . .	8
2.2.3 The design of sensitivity analysis - from grassland to forest . . . . .	10
2.3 Analysis strategy . . . . .	11
<b>3 Results</b>	<b>12</b>
3.1 LES validation - comparison to the observations . . . . .	12
3.1.1 Surface fluxes . . . . .	12
3.1.2 Clouds evolution . . . . .	13
3.2 The effects of coupling the land surface model - including the interactions . . . . .	15
3.2.1 Surface . . . . .	15
3.2.2 Clouds evolution . . . . .	16
3.3 The effects of deforestation - from grassland to forest . . . . .	19
3.3.1 The cloud cover and fraction . . . . .	19
3.3.2 Cloud layer energy release, inhibition and stability . . . . .	21
<b>4 Discussion</b>	<b>27</b>
4.1 Cloud distribution . . . . .	27
4.2 Cloud liquid water . . . . .	29
4.3 Energy release and inhibition in the cloud layer . . . . .	29
4.4 Stability in the cloud layer . . . . .	30
<b>5 Conclusions</b>	<b>33</b>
<b>Acknowledgements</b>	<b>36</b>

<b>References</b>	<b>39</b>
-------------------	-----------

<b>A Supporting figures for the sensitivity analysis</b>	<b>40</b>
--	-----------

## List of Figures

1	Monthly averaged and prescribed profiles of $\theta$ and $q_t$ . . . . .	8
2	Surface sensible and latent heat flux evolution . . . . .	12
3	The comparisons of the $\theta$ and $q_t$ profiles between the observations and LES . . . . .	13
4	Boundary layer heights and cloud evolution . . . . .	14
5	The comparisons of $\theta$ and $q_t$ between off- and online . . . . .	16
6	The comparisons of $q_l$ , $\overline{w'\theta'}$ and cloud fraction between the off- and online . . . . .	17
7	Comparisons of cloud properties between off- and online . . . . .	18
8	Online cloud fraction, LWP and boundary layer height evolution . . . . .	20
9	Online cloud cover evolution . . . . .	21
10	Box plots of cloud properties . . . . .	22
11	Stability evolution . . . . .	23
12	Online temporal evolutions of sensible and latent heat flux . . . . .	40
13	Online temporal evolution of net radiation . . . . .	40
14	Skin temperature . . . . .	41
15	Online cloud fraction, LWP and boundary layer height evolutions . . . . .	41
16	Box plots of cloud properties . . . . .	42
17	Cloud temperature evolutions . . . . .	43
18	Cloud layer inversion . . . . .	43

## List of Tables

1	LES offline initial settings . . . . .	7
2	LES online control initial settings . . . . .	9
3	LES settings of sensitivity analysis . . . . .	10
4	Stabilisation properties of cloud and surface . . . . .	24
5	Stabilisation properties of other variables . . . . .	25

# 1 Introduction

Amazon rainforest is of great importance on earth due to its large area of rainforest. It plays an essential role in the Earth's biosphere (Collow, Miller, and Trabachino 2016) and climate (Hilker et al. 2015). One of the reason is that the Amazon rainforest is a very large carbon sink and can process twice faster than anthropogenic fossil fuel emissions (Phillips et al. 2009). It used to store 120 Pg of carbon in the biomass (Phillips et al. 2009). However, the deforestation has occurred in recent years and more than 10.5% (426,000 km<sup>-2</sup>) of the Brazilian rainforest has been cleared by deforestation (Saatchi, Soares, and Alves 1997) and it also caused changes in vegetation cover and reduction in the leaf area (Hilker et al. 2015).

Because of the removal of forest by deforestation, the surface albedo increases (Quesada, Arneht, and Noblet-Ducoudré 2017), roughness length decreases (Khanna and Medvigy 2014) and LAI decreases (Hilker et al. 2015) consequently. With those changes, the diurnal variability and the boundary layer processes are affected due to the deforestation effects. Since the surface and the atmosphere are closely connected, the changed land characteristics have impacts on the shallow cumulus clouds. This is because the surface controls the essential elements for the shallow cumulus clouds formation, and they include the thermal and moisture content (Vilà-Guerau de Arellano et al. 2014). The turbulence, on the other hand, helps to transfer the thermal and moisture to the atmosphere which can be used for the clouds formation.

Shallow cumulus clouds are essential to the Earth because they strongly influence surface conditions and atmospheric processes, although they only cover 10-25% of the sky (Siebesma et al. 2003). Shallow cumulus clouds affect the surface through their shading and transporting effects. They lower the surface temperature, sensible and latent heat fluxes (Horn et al. 2015). From a dynamical viewpoint, their presence enhances the vertical transport of heat, moisture and momentum to the lower troposphere which may help develop deep convection (Siebesma et al. 2003). From another perspective, the shallow cumulus clouds are strongly influenced by the surface conditions because the surface provides the essential thermal and moisture content for the shallow cumulus clouds formation (Vilà-Guerau de Arellano et al. 2014). As deforestation alters the surface by changing the characteristics, and consequently affects the thermal and evapotranspiration. Therefore, it is important to study the effects deforestation on the shallow cumulus clouds.

Several studies have investigated the relation between the deforestation and shallow cumulus cloud in the Amazon rainforest. Durieux, Machado, and Laurent (2003) used the satellite data and found more low level cumulus clouds with deforestation in the Amazon rainforest. Similar results were found by Wen-Jian and Hai-Shan (2013), and Dickinson and Kennedy (1992). Wang et al. (2009)

also used satellite data but focused on the heterogeneity of the forest when deforestation occurred. They identified that shallow cumulus clouds occurred more over deforested areas than the forest because of the changing of surface properties. Apart from the total effects of deforestation, several variables related to the role of surface properties have been investigated individually as well. Ek and Holtslag (2004), discovered that less stability above the boundary layer and drier soil would give rise to more shallow cumulus clouds by using the observations and the Coupled Atmospheric Boundary Layer Plant-Soil (CAPS) model. Their study also gave indications for the relationship between the stability in the cloud layer and cloud cover. Furthermore, Park, Böing, and Gentine (2018) used the Large-Eddy Simulation (UCLA-LES) and concluded that a greater roughness length resulted in more low level clouds. Cloud liquid water path (LWP), on the other hand, represents the liquid water content of the clouds. It was found to be decreased by deforestation by Nair et al. (2003) who used the Regional Atmospheric Modelling System.

In addition to the changes in the occurrence of shallow cumulus clouds, the energy release and inhibition in the cloud layer are also affected by the deforestation. The Convective Available Potential Energy (CAPE) and Convective Inhibition (CIN) are the representation of those two forms of energy. In the study of Yin et al. (2015), they found an overall greater value of CAPE with wetter soil. Wang et al. (2009) discovered a stronger CAPE in the forest region when studying the heterogeneity with the deforestation using the observations because of a greater humidity. CIN, on the other hand, was found to be negatively related to the convective boundary layer height due to the effects of a stronger inversion (Kalthoff et al. 2011).

Extending on these studies, this research investigates how the atmosphere interacts with the land surface during dry season in Amazon rainforest. It also examines how the shallow cumulus clouds are affected. The dry season is chosen because with less precipitation, we can eliminate a complicated factor and focus on the land-surface interactions. The methodology of this study is based on the combination of three numerical experiments constrained by the observations from K34 forest station near Manaus, in Brazil (September, 2014). The usage of radio soundings is important because a lot of studies did not include it whereas it can connect the surface to the atmosphere. In addition to the observations, the Dutch Atmospheric Large-Eddy Simulation (LES) model is used for this study in order to investigate the effects deforestation (Heus et al. 2010). LES is a useful model because it explicitly resolves the turbulence related to the clouds formation and can add interactions to the land-atmosphere system by coupling a land surface model. This is important as well, because most of the aforementioned studies used large scale models and satellite data, with only Park, Böing, and Gentine (2018) using the LES. However, Park, Böing, and Gentine (2018) only studied the effects of roughness length which accounted for one part of

deforestation. Therefore, this study examines the deforestation from three perspectives and use the LES to investigate the shallow cumulus clouds in the Amazon rainforest during the dry season.

However, this study does not focus on the heterogeneity with deforestation in the Amazon rainforest or deep convection, because we average the entire domain and only focus on the formation of shallow cumulus cloud with shallow but not the deep convection.

Using the combined methodology, the research questions are as follows:

- What is the response of shallow cumulus clouds to an explicit coupling to the land surface properties?
- What are the effects of changing the values of albedo, roughness length and LAI from grassland to forest on the shallow cumulus clouds?

In order to answer the research questions, the starting point of this research is to present a typical day during the dry season by averaging the data for all 30 days in September. Obtaining the 30-day average is important because it shows the typical diurnal variability of the thermals and the moisture in a dry-season month. The averaged diurnal evolutions include sensible heat flux, latent heat flux and the vertical profiles of potential temperature and specific humidity. Those variables are used for the initial input of LES, and the LES is validated to represent a realistic surface and an atmospheric boundary layer observed during the dry season in the Amazon rainforest.

Following the analysis of the observations, we design a suit of numerical experiments using the LES. The first two are the control runs with and without a coupled land surface. Both of them are validated by the 30-day averaged observations. For the second set of the experiment we have the surface properties of a grassland. Then a sensitivity analysis is conducted by changing the surface properties from grassland to forest and this is achieved systematically by changing the values for albedo, roughness length and LAI. The three variables are first altered separately in order to check the sensitivity of shallow cumulus clouds to each of them and then they are combined to represent the forest. The prescribed settings in the study of Vilà-Guerau de Arellano et al. (2011) for the LES provide some inspirations for this research to define the initial model setup for the boundary layer, as some parameters at the beginning of the simulations are borrowed from their study. In this study, we analyse the energy fluxes, the boundary layer evolution and the cloud properties.

This paper is organised as follows: The methodology is shown in the next section where the observations and the LES are introduced in detail. It is followed by the results section. The fourth section discusses the results and compares them to the previous studies. It also gives the recommendations for future studies. In the last section, conclusions are drawn.

## 2 Methodology

This section introduces the overall methodology of the research. It mainly uses the observations from the Amazon rainforest and the Dutch Atmospheric Large-Eddy Simulation (DALES). For simplicity, this paper will refer to LES from now on. Overall, three experiments of LES are designed to answer the research questions above. Then, the model validation is introduced and the model is validated by the observations from K34 meteorological station in the Amazon rainforest in order to simulate the real atmospheric boundary layer conditions. Finally, the analysis strategy is introduced for the entire study.

### 2.1 Datasets

To study the Amazon shallow cumulus clouds formation, the dry season month September, 2014 is chosen to represent the real situations. As there is normally less precipitation in the dry season, it is more likely to focus on the shallow cumulus clouds. The September is drier than the wet-season months in 2014 with small variabilities in boundary layer conditions. The location of this study centres around the K34 meteorological tower in the Amazon rainforest, near Manaus, Brazil ( $2^{\circ}36'32.67''\text{S}$ ,  $60^{\circ}12'33.48''\text{W}$ ). It is also the place where the observations are obtained. This tower is surrounded by a homogeneous broadleaf evergreen rainforest, thus it is a good representation for the undisturbed Amazon rainforest.

The variables measured in K34 include time evolutions of surface variables and vertical profiles from the radio soundings. All the data were obtained from the Green Ocean Amazon Experiment (Martin et al. 2017). The most important ones obtained from the surface are sensible and latent fluxes, as they determine the base of heat and moisture in the bottom of the boundary layer for this study. Apart from the fluxes, the vertical profiles from the radio soundings are essential as well, because they link the surface to the atmosphere, a level where clouds occur. The radio soundings used in this research consist of height, temperature, pressure and relative humidity. With these data, we are able to obtain the vertical profiles of potential temperature and specific humidity. The data from radio soundings is collected five times everyday, and the times are 1:30 LT, 7:30 LT, 10:30 LT, 13:30 LT, and 19:30 LT. However, only the data from 1:30 LT is used as model input and the rest are applied to the model validation.

As we aim to set a typical dry season day in the Amazon rainforest, all the data from September are taken into account by averaging. After the averaging, clear sinusoidal evolution are found for both sensible and latent heat flux (Figure 2). The profiles from the radio soundings show typical vertical variations at different time as well. For instance the profiles at 1:30 LT are similar (Figure 1) and

have the characteristics of a stable nocturnal boundary layer.

Apart from representing a typical dry season day in the Amazon rainforest, the observations are used to validate the LES. The LES is validated with the averaged sensible and latent heat flux from the surface. Meanwhile, it also uses the profiles of the averaged observations of potential temperature and specific humidity at 1:30 LT for the initial model input at the beginning of the experiments.

## 2.2 Experimental Design

In our study we use LES for conducting several experiments (Heus et al. 2010). Since LES has explicit calculations of fluxes and high resolutions in meters, it performs well in representing the processes in the scales of a few hundred meters, such as shallow cumulus clouds. The representation is achieved by applying the monthly averaged sensible heat flux, latent heat flux, vertical profiles of specific humidity and potential temperature to the LES. These variables are used because they are closely related to the formation of shallow cumulus clouds and are analysed in this study. In one of the steps, we couple the LES to a land surface model which not only enables land-atmosphere interactions, but can also change the vegetation cover from grassland to forest. However, since LES has high computational cost due to the explicit calculations, thus, it focuses on a small area and some larger scale processes are neglected.

With the model and observations, three experiments are performed:

- Offline grassland: the LES uses prescribed values for the diurnal evolution of sensible and latent heat flux and profiles of potential temperature and specific humidity for the initial setup. It assumes no interaction between atmosphere and surface. Note that these initial setups will be validated according to the averaged observations and the initial model results.
- Online grassland control (G): the land surface model is switched on to allow interactions and the vegetation cover characteristics are set according to a grassland. The variables that represent the grassland are albedo, roughness length and LAI. This experiment is validated by the sensible and latent heat flux from the offline experiment.
- Online forest: the land surface model will also be used and the parameters regarding the deforestation will be changed to forest properties. The steps are as follows:
  - Forest Albedo (A-): The albedo is lowered and others remain the same;
  - Forest Roughness Length (RL+): The roughness length is greater and the others remain the same;

- Forest LAI (L+): The LAI is made greater and the others stay unchanged.
- Forest (F): This experiment combines all the changes of albedo, roughness length and LAI.

The simulation period is the September, 2014 for the LES, as September is one of the dry season months (Anber et al. 2015). Furthermore, the referencing study by Vilà-Guerau de Arellano et al. (2011) was also carried out in September, 2014 and more details can be found from their paper.

### **2.2.1 Initial LES model setup - offline**

Since the LES model needs input from the historical boundary layer conditions, the initial conditions from the model need to be validated by the observations in order to obtain a typical dry season day conditions. This study takes into account all thirty days from September, 2014 in order to obtain the typical boundary layer conditions of a dry season day in the Amazon rainforest. Additionally, the standard deviations are calculated to set the trusted ranges of all observed variables. Therefore, the validation includes diurnal variations of sensible heat flux, latent heat flux, the initial profiles of potential temperature and specific humidity. The overview of all prescribed and initial settings can be found from Table 1. The validated variables (potential temperature, specific humidity, sensible heat flux and latent heat flux) are used as LES model input. Other LES model setups are explained more in detail in the study of Vilà-Guerau de Arellano et al. (2011).

The model validation started from the analyses of the observations from K34 in the Amazon rainforest. Monthly averages of surface fluxes and the mean profiles are calculated at 1:30 LT, 7:30 LT, 10:30 LT and 13:30 LT respectively. The sensible heat flux, latent heat flux and the profiles at 1:30 LT define the initial boundary layer conditions of the LES.

Surface fluxes are indicated by Figure 2, in which the observations of sensible and latent heat flux show clear sinusoidal variations. The prescribed sensible heat flux curve (Figure 2.a) is slightly higher than the observations at the beginning in order to add more buoyancy and obtain more active shallow cumulus clouds. The rest of the evolution follows the observations. The sensible heat flux starts to increase after the first hour of the simulation (after 7:00 LT) and becomes zero after around ten hours (at 16:10 LT). On the other hand, the prescribed latent heat flux (Figure 2.b) closely follows the observations and it increases at the same time as sensible heat flux but reaches zero at the end of the simulation. Although deviations exist between the observed and prescribed surface fluxes, the prescribed variations are designed as close as they can to stay in the range of standard deviations indicated by the shades in Figure 2.

Table 1: The initial prescribed settings for offline LES experiment

Properties	Value
<b>Boundary Layer Properties</b>	
Large scale subsidence velocity $w_s$ [ $\text{m s}^{-1}$ ]	0
Wind speed [ $\text{m s}^{-1}$ ]	0
<b>Heat</b>	
Surface sensible heat flux (offline) [ $\text{K m s}^{-1}$ ] (from 6:56 to 18:00 LT)	$\overline{w\theta_s} = 0.114 \sin\left(\frac{\pi(t-3600)}{33000}\right) + 0.0006$
Potential temperature profile [K]	
$z < 50$ m	297
$50 < z < 590$ m	$297 + 0.0129(z - 51)$
$590 < z < 2010$ m	$304.2 + 0.002(z - 750)$
$2010 < z < 2810$ m	$306.8 + 0.007(z - 2010)$
$z > 2810$ m	$312.3 + 0.03(z - 2800)$
<b>Moisture</b>	
Latent heat flux (offline) [ $\text{g}_w \text{ kg}_a^{-1} \text{ m s}^{-1}$ ] (from 07:00 to 17:00 LT)	$\overline{wq_s} = 1.43 * 10^{-1} \sin\left(\frac{\pi(t-3600)}{36000}\right)$
Specific moisture profile [ $\text{g}_w \text{ kg}_a^{-1}$ ]	
$z < 130$ m	16.16
$130 < z < 2810$ m	$15.16 - 0.00296z$
$z > 2810$ m	$22.43 - 0.0056z$

Apart from the surface fluxes, the initial profiles of the potential temperature and specific humidity are also prescribed for the model validation. Figure 1 indicates the observations, the prescribed curves and the ranges of standard deviations calculated from the observations. Inspired by the observations at 1:30 LT, the prescribed profiles for the potential temperature and specific humidity are presented by the black solid lines in Figure 1. The potential temperature at the surface is kept constant at 297 K. Above the surface and below 590 m, the potential temperature follows the observations and increases with a constant lapse rate at  $0.0129 \text{ K m}^{-1}$ . Above 590 m, the prescribed potential temperature profile almost overlaps the observations until 2010 m. A smaller lapse rate helps trigger more unstable boundary layer and enables buoyancy flux to rise to a higher level which makes the shallow cumulus clouds less passive. The lapse rate above 2010 m again increases to control the clouds from overcasting. However, the slight increase of the lapse rate between 2010 m and 2800 m is not enough to constrain the moisture from reaching a higher level and leaving almost no clear sky from above. Therefore, a greater lapse rate  $0.03 \text{ K m}^{-1}$  is designed above 2810 m to

achieve a partly cloudy sky.

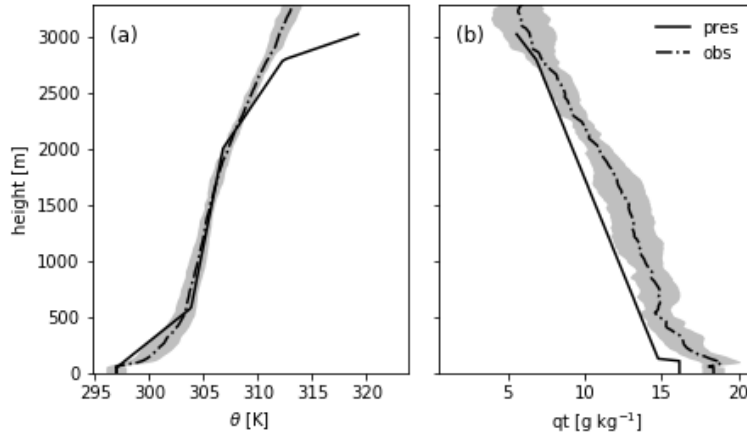


Figure 1: The initial (a) potential temperature and (b) specific humidity profiles. The dashed lines indicate the averaged observations at 1:30 LT and the black curves are the prescribed profiles regarding the observations which are used in the offline experiment. The shades show the ranges defined by the standard deviations of the observations at 1:30 LT.

Simultaneously, the prescribed specific humidity has a similar trend with the observations although they do not overlap. Similar to the potential temperature, the specific humidity also has a constant value of  $16.16 \text{ g kg}^{-1}$  at the surface. Then, the specific humidity jumps to  $15.16 \text{ g kg}^{-1}$  and starts to decline  $0.3 \text{ g kg}^{-1}$  every one hundred meters with height until 2810 m where it decreases faster to control the cloud top and cover. Overall, the prescribed specific humidity is shifted leftward to the observations because the cloud cover will reach 100% if it overlaps the observations, which does not present the shallow cumulus clouds. Therefore, the prescribed specific humidity is smaller to prevent such situation.

Although the prescribed curves are slightly different from the mean observations, they are still close to or in the range defined by the standard deviations for both surface fluxes and the vertical profiles (Figure 2 and 1). Therefore, the prescribed curves do follow the observation trends except for the part above 2810 m which is specially designed for capping the cloud top.

### 2.2.2 The setup of Land Surface Model - online grassland control

The numerical settings of this experiment are similar to the previous one but the LES is coupled to a land surface model to enable the interactions between the atmosphere and the surface. The difference between the two experiment is that the sensible and latent heat flux are generated by the LES which depends on the land surface model. Therefore, other variables are added or adjusted

to obtain an online-grassland-control. They are designed to validate the evolution of sensible and latent heat flux obtained from the averaged observations. The related variables are set in an input file of the LES (Table 2). This experiment includes the Ags for interactive CO<sub>2</sub> fluxes and resistance.

Table 2: The initial settings for online grassland control based on the offline experiment

Items	Values/Settings
<b>Location and Time</b>	
Coordinates	(2.6091 S, 60.2093 W)
Day of the year (Sept. 10 <sup>th</sup> )	253
Start time of the simulation (LT)	6:00
<b>Soil Properties</b>	
Soil temperature [K]	
tsoilav (1-2)	294
tsoilav (3)	295
tsoilav (4)	296
Soil porosity [m <sup>3</sup> m <sup>-3</sup> ]	0.5
Wilting point [m <sup>3</sup> m <sup>-3</sup> ]	0.171
Soil moisture at field capacity [m <sup>3</sup> m <sup>-3</sup> ]	0.4
Soil moisture phiwav (1-4) [m <sup>3</sup> m <sup>-3</sup> ]	0.3
Root fraction [-]	
rootfav (1)	0.35
rootfav (2)	0.38
rootfav (3)	0.23
rootfav (4)	0.04
<b>Surface Properties</b>	
Roughness length [m]	0.05
Albedo [-]	0.25
Vegetation cover [m <sup>2</sup> m <sup>-2</sup> ]	0.9
LAI [m <sup>2</sup> m <sup>-2</sup> ]	2
Heat capacity at skin layer [J K <sup>-1</sup> m <sup>-2</sup> ]	10000
Heat conductivity at skin layer [J s <sup>-1</sup> K <sup>-1</sup> m <sup>-2</sup> ]	12
<b>Boundary Layer Properties</b>	
Wind speed [m s <sup>-1</sup> ]	1
<b>Land Surface Model</b>	
Interaction scheme (using radiation)	A-g <sub>s</sub> resistance calculation
Use simple surface radiation for land surface model	A-g <sub>s</sub> CO <sub>2</sub> fluxes calculation

The changes in location and time section from Table 2 result in four hours' difference between the local and universal time. Therefore, the starting time of the LES should be set as ten. In addition to the basic settings, several variables of surface properties are adjusted to make the simulation close to the offline experiment. For example, roughness length is made slightly greater and heat conductivity at skin layer is greater as well in order to fit the diurnal variations of sensible and latent heat flux to the offline. The soil temperatures are related to the surface temperature measured in the Amazon rainforest as well. Moreover, the LES switches the surface parameterisation from the forced values to interactive scheme by using the radiation variations. To achieve the interactions, the LES is coupled with a land surface model with the simple surface radiation (Heus et al. 2010). Apart from coupling the land surface model, some other soil and surface properties are added as well (Table 2). The soil temperature gradients, soil water content and root fraction are added to the LES in this experiment. The combination of them connects the soil to the surface. The results of this experiment are used as a basis for coupling the land surface model with LES. In all the online experiments, the initial soil moisture index is set at 0.56 and note that cloud shading effects are not included. The soil moisture index is calculated as follows:

$$\frac{sm - wp}{sc - wp}, \quad (1)$$

where *sm* is the soil moisture, *wp* is the wilting point and the *sc* represents soil moisture capacity.

### 2.2.3 The design of sensitivity analysis - from grassland to forest

Based on the online grassland control, the sensitivity analysis changes the albedo, surface roughness length and LAI to forest values. In this section, four experiments are designed. They are Forest Albedo (A-, smaller albedo), Forest Roughness Length (RL+, greater roughness length), Forest LAI (L+, greater LAI) and Forest. In the first three steps, the variables are changed to the corresponding

Table 3: The settings for sensitivity analysis based on the online grassland control

Simulation	Albedo [-]	Roughness length [m]	LAI [m <sup>2</sup> m <sup>-2</sup> ]
Grassland (G)	0.25	0.05/0.01	2
Forest Albedo (A-)	0.15	0.05/0.01	2
Roughness Length (RL+)	0.25	0.5/0.1	2
Forest LAI (L+)	0.25	0.05/0.01	5
Forest (F)	0.15	0.5/0.1	5

\*Shaded cells represent the changed values of each experiment from the Grassland.

forest values separately, whereas the last one combines all three to represent the forest experiment. Table 3 shows the specific settings for the sensitivity analysis and in which, the 'Grassland' is the 'online grassland control' and it stays here for reference.

### **2.3 Analysis strategy**

The analysis starts from comparing the offline model results and the observations. First of all, the diurnal evolution of sensible and latent heat flux are compared for checking the basic model simulation. It is followed by comparing the vertical profiles from the LES and the observations. Then the boundary layer height, cloud base and top are compared to the observations as well. In this step, the boundary layer heights are found where the maximum vertical gradients of potential temperature occur and the cloud top is estimated using the parcel method. For better comparisons, the boundary layer height from the LES results are calculated using the maximum potential temperature gradient as well.

In order to find the effects of including the interactions in the system, previous analyses are also used, although more steps are taken. Additionally, profiles of liquid water mixing ratio, buoyancy flux and cloud fraction at different times are plotted for the comparisons. Finally, the time evolution of cloud depth, cloud cover and liquid water path are compared to find the differences. From this part of the sensitivity analysis on, the boundary layer height is calculated using the minimum buoyancy flux because it gives a clearer signal for the heights.

In analysing the effects of deforestation, the main focus is on the cloud properties. It includes three parts: the horizontal distribution of the clouds, the vertical content of the cloud liquid water and the cloud energy. Firstly, the analysis shows the direct results of deforestation by comparing the grassland and forest. Then, the results from the intermediate steps are checked to find the sensitivity of clouds to each deforestation-related variable. Finally, depending on the period of cloud cover when it reaches the maximum and stays rather constant, the data distribution of the variables are analysed in those periods against the evaporative fraction. Here, the evaporative fraction is used because it represents well the ratio of latent heat flux to the available energy and helps find the effects of moisture content in the energy partitioning.

### 3 Results

In this section, the results from all experiments are presented in the order of the designed experiments. Firstly, this section shows the comparisons between the model results from the first two experiments and the observations. Then it is followed by the analyses of the effects after activating the land-atmosphere interactions. The experiments which switch from grassland to forest are presented at the end.

#### 3.1 LES validation - comparison to the observations

##### 3.1.1 Surface fluxes

Since shallow cumulus clouds are strongly influenced by the surface, the sensible heat flux and latent heat flux are the first to be analysed. This is because they represent the important turbulent energy and moisture conditions for the clouds formation. Therefore, the evolution of both variables is examined in this section.

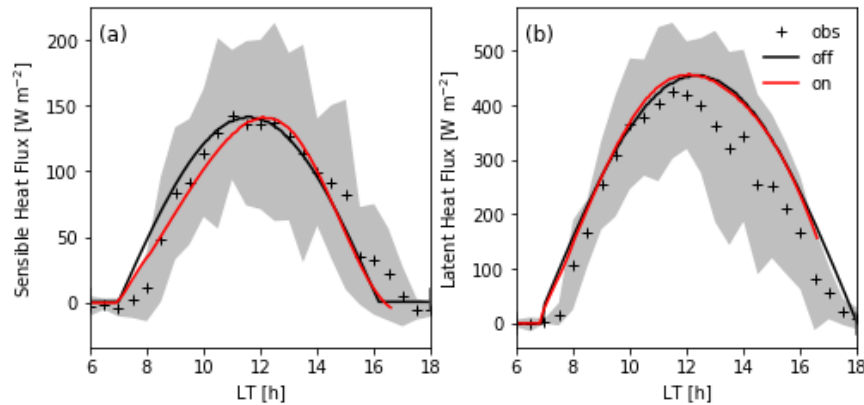


Figure 2: The temporal evolution of sensible (a) and latent heat flux (b) from the averaged 30-day observations (black crossings '+'), the offline (black) and the online grassland control (red) experiments. The shadows are twice the standard deviations from the observed sensible and latent heat flux. The four vertical grey lines indicate the start and end time of the experiment.

With the initial settings, the LES ran for twelve hours from 6:00 to 18:00 LT. The two plots in Figure 2 indicate the diurnal evolution of sensible and latent heat flux from both the observations and LES experiments. All curves of sensible and latent heat flux are almost in the range defined by the standard deviations from the observations. This implies good validation of LES by the actual boundary layer at the surface.

Figure 2.a shows that the sensible heat flux of the two experiments starts to increase at 7:00 LT and

becomes zero at 16:00 LT which is before the observations. The slightly earlier development of sensible heat flux may initiate the development of the boundary layer earlier from the LES than the observations. The two experiments - offline and online have similar variations.

Latent heat flux of the two experiments, on the other hand, deviates more from the observed values especially after 12:00 LT and it has generally greater values. Figure 2.b shows an earlier increase and later silence of latent heat flux, therefore, more moisture is evaporated and carried to the atmosphere. Two experiments almost overlap except for the earlier ending of the online experiment at around 16:00 LT as the sensible heat flux becomes zero at the moment.

Since the comparisons in this subsection are not enough to confirm the quality of validation, more data should be analysed about cloud properties. However, the observations do not have any direct observations for the cloud. Therefore, the profiles from the radio soundings are used to estimate the boundary layer height and the cloud top. The boundary layer height is found by the maximum potential temperature gradients and the cloud top is estimated by the parcel method. They are shown in the next subsection.

### 3.1.2 Clouds evolution

Apart from the surface heat fluxes, the vertical profiles of potential temperature and specific humidity give indications of vertical evolution of heat and moisture which are related to the shallow cumulus clouds formation. The cloud base, top and the boundary layer height can be found from the radio soundings as mentioned. Consequently, they help evaluate the LES validation.

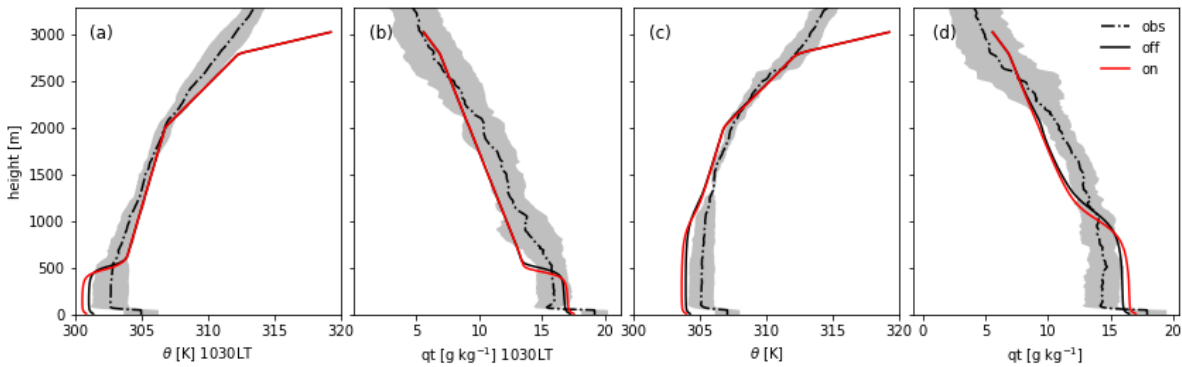


Figure 3: The profiles of potential temperature (a & c) and specific humidity (b & d) at 10:30 LT and 13:30 LT. The solid lines are the LES results from both the offline (black) and online (red) experiments, the dashed lines are the averaged 30-day observations and the shades represent twice the standard deviations.

The observations and LES results of profiles at 10:30 LT and 13:30LT are selected. This is because

at 10:30 LT, the shallow cumulus clouds start to initiate although no clouds can be found, whereas at 13:30 LT, the clouds appear above the boundary layer. Their combination shows the LES validation from both clear and partly cloudy sky. The comparisons of the LES results and the observations of potential temperature and specific humidity profiles at 10:30 LT (local time) and 13:30 LT are shown in Figure 3. At 10:30 LT, an unstable boundary layer has the depth about 600 m with an inversion at around 3 K. Whereas, at 13:30 LT, the unstable boundary layer grows to 1200 m with a higher surface temperature (Figure 3.c) and the inversion is 2 K smaller at 13:30 LT.

The simulated profiles more or less fall into the ranges defined by the standard deviations. The results which are outside the standard deviation represents only a small part of the profiles. However, the LES generated stronger inversions (1-2 K more) than the real boundary layer (Figure 3.a and b) and the inversion is stronger at 10:30 LT than at 13:30 LT from the LES. Since larger inversions do not encourage entrainment or boundary layer growth, the clouds are barely seen at 10:30 LT from the model results. Since at 13:30 LT, the boundary layer heights of both offline and online experiments are similar, the validation for both experiments are well validated. Additionally, both experiments resulted in a colder and moister boundary layer than the observations which implies shallow cumulus clouds with lower bases but larger sizes and depths. Therefore, a conclusion can be drawn here that the LES has been well validated by the observations and the results from the LES experiment prove themselves as reliable.

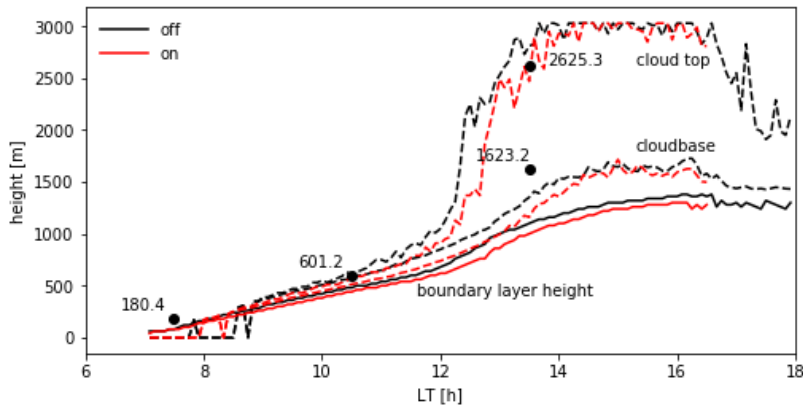


Figure 4: Time evolution of boundary layer height (solid lines), cloud base and top (dashd lines) from the offline (black) and online (red) experiments. The four black dots in (a) indicate the boundary layer heights estimated from the observations at 07:30 LT, 10:30LT, 13:30 LT and the cloud top at 13:30 LT. The estimation uses the parcel method for the cloud top and the maximum gradient of potential temperature profiles for the boundary layer height.

In terms of giving the indications for shallow cumulus clouds, Figure 4 presents some more direct

information. The lower three black dots are the calculated boundary layer heights from the observed profiles of potential temperature using the greatest vertical gradient of potential temperature. Whereas, the upper one is the cloud top at 10:30 LT. It is found at the level of the limit of convection by using the parcel method which applied the dry and moist adiabats according to the observed surface temperature and moisture. As can be seen from the figure, the simulated boundary layer heights are close to the simulated ones at 7:30 LT and 10:30 LT, but are lower than the observed ones because the LES generated greater inversions. The cloud top is higher than the estimated one and it makes the cloud depth larger since the LES introduced more moisture content and heat to the system as is indicated in Figure 2.

### **3.2 The effects of coupling the land surface model - including the interactions**

This section will demonstrate the effects of adding the interactions between the land and atmosphere, namely it states the differences between the offline and the online experiments. This section first compares the sensible and latent heat flux as a representation of the surface properties. Then the vertical profiles of potential temperature, specific humidity, the time evolution of the boundary layer height and the cloud properties are presented afterwards.

#### **3.2.1 Surface**

In the offline experiment, the sensible and latent heat fluxes are prescribed for the LES. Whereas, after the LES is coupled with the land surface model, the LES defines its own flux evolution depending on the land-atmosphere interactions which can be partly controlled by the variables in Table 2. The variables from Table 2 are revised to be validated by both the averaged sensible and latent heat flux from the offline experiment. Therefore, after the validation, the differences between the two experiments are small.

As can be seen from Figure 2, both experiments are similar to each other, although some deviations between the offline and the online experiments are observable. Before 12:00 LT, the sensible heat flux of the online experiment increases slightly slower than that of offline. However, the total deviations of sensible heat flux of the two experiments from the observations are small. The slower increase from the online experiment may result in a later development of the boundary layer as the heat energy is less strong. On the other hand, the growth of the boundary layer from the online experiment between 12:00 LT and 14:00 LT is a bit faster than the offline experiment in the same period, although the overall boundary layer evolution is still thinner than the offline. Thus, the clouds have opportunities to even grow larger with the extra amount of buoyancy increase in these two hours. Whereas the total energy is still expected to be less in the online experiment as the

surplus before 12:00 LT does not compensate the deficit after. Contrary to the sensible heat flux, the evolution of latent heat flux for both experiments are almost identical before 16:00 LT, although the model stops shortly after because sensible heat flux reaches zero.

Overall, the latent heat flux for both the experiments is almost the same, whereas the sensible heat flux is smaller in the online experiment. Therefore, the smaller sensible heat flux from the online experiment constrains the amount, size and the height of the shallow cumulus clouds and the boundary layer.

### 3.2.2 Clouds evolution

Again in this section, the profiles of potential temperature and specific humidity, the boundary layer height evolution and the cloud properties are examined at different times. The comparisons between the two experiments are presented to evaluate the effects of the online land-atmosphere system.

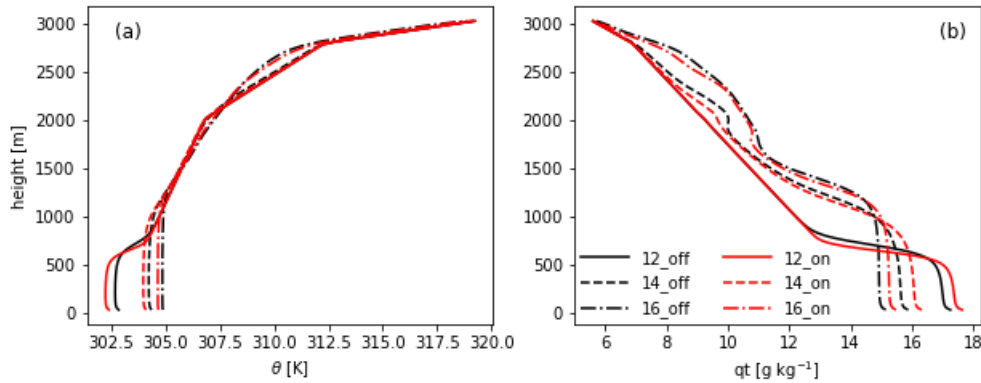


Figure 5: Vertical profiles of (a) potential temperature and (b) specific humidity at 12:00 LT (solid lines), 14:00 LT (dotted dashed lines) and 16:00 LT (broken lines) for both offline (black) and online (red) experiments

The vertical profiles of potential temperature and specific humidity show that the online experiment has moister and colder boundary layer (Figure 5). Both two plots indicate the growth of boundary layer height with time. At 12:00 LT, the boundary layer height is around 700 m for both experiments, and it becomes 1200 m at 16:00 LT. The growth of boundary layer height between 12:00 LT and 14:00 LT is greater than the next two hours, because of the faster decrease of sensible heat flux with time in the latter two hours. At those three time points, the offline experiment always has a deeper boundary layer (less than 100 m) due to overall greater sensible heat flux.

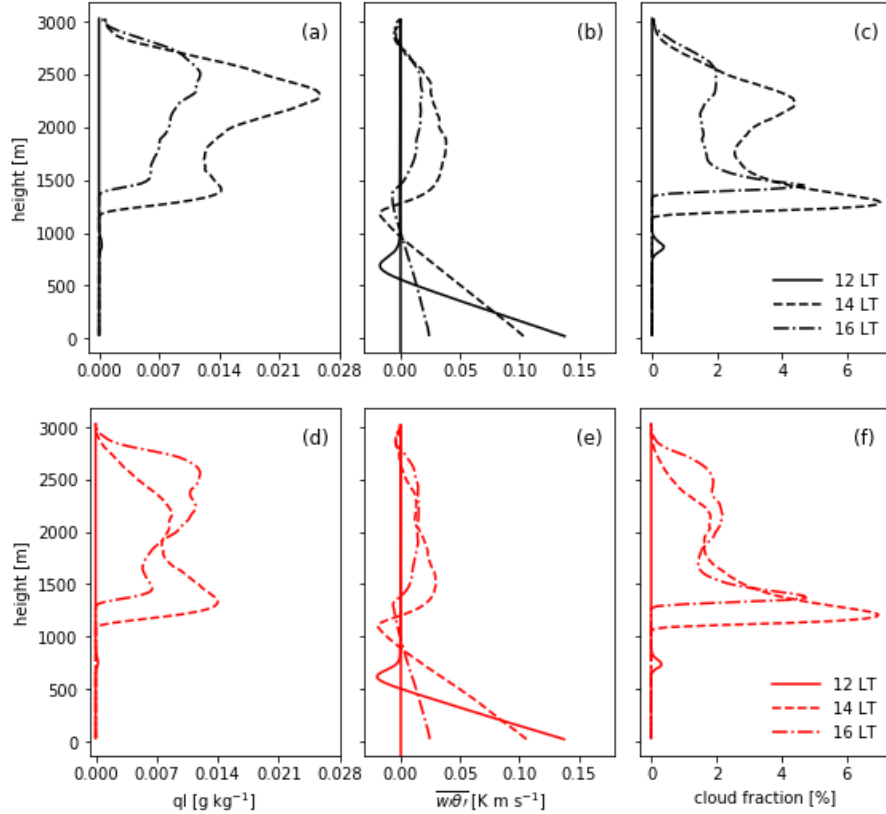


Figure 6: Profiles of liquid water mixing ratio ( $q_l$ ), buoyancy flux ( $\overline{w'\theta'}$ ), and cloud fraction of offline (black, a, b & c) and online experiments (red, d, e & f) at 12:00 LT (solid lines), 14:00 LT (broken lines) and 16:00 LT (dotted dashed lines)

Interestingly, in the offline experiment, the surface is wetter in the online experiment even though the latent heat flux evolution is almost identical for the both. To explain this gap between the experiments, we need to zoom in on Figure 2.b. From 10:00 LT to 12:00 LT, there are some small differences between the two experiments. The latent heat flux from the online experiment is approximately  $10 \text{ W m}^{-2}$  greater than the offline, which may introduce more moisture to the boundary layer during this period. However, as the time moves on, the differences among the profiles become smaller with time in the online experiment. This small gap of the latent heat flux can be related to the response of stomatal conductance of plants with temperature since the land surface model has the active vegetation response. As normally, temperature starts to increase in the morning and reaches a peak shortly after noon. Stomata, which are greatly affected by the temperature, tend to close with higher temperatures to prevent from more transpiration (Avisar et al. 1985). Apart from temperature, radiation is also an indirect factor to make the stomata open. In the morning, incoming radiation starts to increase rapidly, which increases the temperature and

causes the stomata to open. Then, the transpiration is enhanced in the morning. Therefore, due to the coupling of land surface model, the latent heat flux is greater before noon, and when the stomata close after noon, latent heat flux decreases more and follows the prescribed curve.

Other profiles of liquid water mixing ratio, buoyancy flux and cloud fraction are more direct to the represent the shallow cumulus clouds. The comparisons between the offline and online experiments can be clearly observed in Figure 6.

The liquid water mixing ratio of online experiment is significantly lowered at 14:00 LT and slightly enlarged at 16:00 LT (Figure 6.a & d). Similar conditions can also be found for buoyancy flux and cloud fraction (Figure 6.b, c, e & f). Thus, at 14:00 LT, the cloud size is smaller in the online experiment and a bit larger at 16:00 LT. Similar phenomena can be found from the buoyancy and cloud fraction as well by observing the positive part of the profiles. However, the difference is that the cloud-size changes are small with time from the online experiment especially between 14:00 and 16:00 LT comparing to the offline experiment. The cloud-size variations can be explained by the variations of sensible and latent heat flux. This is because the slightly larger sensible heat flux during this period with enough moisture supply makes sure that the clouds do not dissipate very fast.

Since the bottom lines of both liquid water mixing ratio and cloud fraction represent the level where their values start to change significantly with height, the cloud base can be found at these levels. By observing those heights, it confirms that the shallow cumulus clouds generally have lower cloud base from the online experiment and it corresponds well to the lower boundary layer height from Figure 4 and 5. The lower cloud base is because a smaller sensible heat flux at the beginning and almost identical latent heat flux result in a lower boundary layer height.

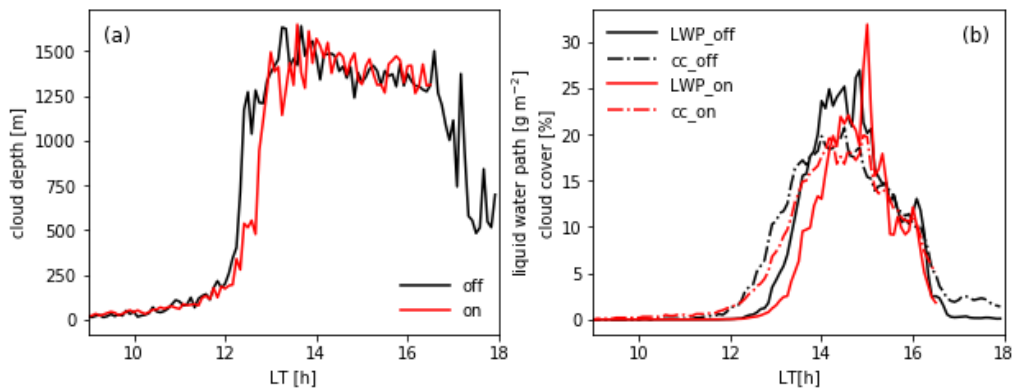


Figure 7: Time evolution of (a) cloud depth, (b) liquid water path (LWP, solid) and cloud cover (cc, dashed) from the offline (black) and online (red) experiments.

Apart from the temporal evolution, the profiles of potential temperature and specific humidity can explain the clouds properties as well. At the beginning of the simulation, the profiles of potential temperature and specific humidity are similar to the initial prescribed profiles. Whereas at 12:00 LT, the differences of those variables at the surface are observable. A colder boundary layer and a greater inversion shown in the profiles negatively affect the shallow cumulus clouds formation. Under those conditions, the clouds are more passive and thus smaller and lower in the online experiment.

Comparing to the smaller sensible heat flux from the online experiment, the slightly greater latent heat flux (less than  $10 \text{ W m}^{-2}$ ) between 10:00 LT and 12:00 LT does not contribute much to the cloud properties. Surprisingly, given the larger latent heat flux, the cloud cover, depth and the liquid water path (as shown in Figure 7) do not have the expected overall greater values because of a smaller sensible heat flux. The clouds start to develop about half an hour later in the online experiment and the cloud depth is smaller to the offline experiment. Even though the maximum of the liquid water path is greater than that of the offline experiment, for the rest of the time, the liquid water path is still lower due to the smaller values of sensible heat flux in total. It may imply that the greater moisture content has greater contribution to the cloud water density only. If without strong sensible heat, the clouds are less in the online experiment. Thus, the sensible heat flux has a more significant influence on the cloud properties than the latent heat flux.

### **3.3 The effects of deforestation - from grassland to forest**

This section shows the results from the sensitivity analysis. It first compares the results from the grassland and forest experiments. Then, the results from the intermediate steps between the grassland and the forest are presented. In this section, the 'online grassland control' are referred to as 'Grassland' for simplicity.

#### **3.3.1 The cloud cover and fraction**

Figure 8 demonstrates the overall effects of the changed albedo, roughness length and LAI on the cloud fraction evolution (Forest). Generally, more clouds can be observed from the Forest experiment by comparing the two plots in Figure 8. The plots illustrate that both cloud cover and liquid water path are greater in the forest with an earlier appearance, whereas the boundary layer height is lower from Forest experiment than the Grassland. Therefore, both from the time evolution and the vertical distribution of clouds are greater with more liquid water in the Forest experiment.

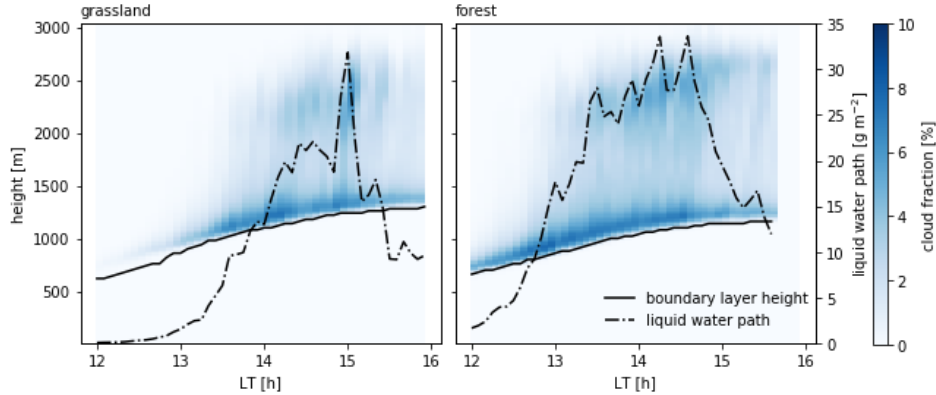


Figure 8: Temporal evolution of cloud fraction (colour band), boundary layer height (black solid lines), and the liquid water path (black dashed lines) of the Grassland (left) and the Forest (right) experiments.

To explain these differences, the changes of albedo, surface roughness length and LAI representing the surface properties should be taken into account. Firstly, a smaller albedo enables more absorption of solar radiation (the maximum increase is  $97.8 \text{ W m}^{-2}$ , Figure 13 from the Appendix), which may result in a greater sensible heat flux because of more available energy. However, the sensible heat flux is smaller from forest than the grassland, because in the Forest scenario the LAI is increased from  $2$  to  $5 \text{ m}^2 \text{ m}^{-2}$ , which accounts for the greater partitioning of energy to latent heat flux (Figure 12). The increase in the latent heat flux can be explained by the enhancement in transpiration due to the greater vegetation cover (Beltrán-Przekurat et al. 2012; Chen et al. 2018). Therefore, more energy is partitioned to the latent heat flux than sensible heat flux in the Forest experiment. Because of a smaller sensible heat flux, the lower boundary layer height from the Forest can be explained. This is because a less strong buoyancy is only able to bring the moisture to a lower level comparing to the Grassland. From the mechanical perspective, a higher surface roughness length should lead to greater turbulence mixing (Khanna and Medvigy 2014). This can be partly reflected on the redistribution of sensible and latent heat flux. With greater roughness length, the sensible first rises faster than the Grassland but becomes smaller at around 13:00 LT. However, the latent heat flux is always greater than the Grassland and the increase is small (Figure 12) possibly due to the small initial wind speed ( $1 \text{ m s}^{-1}$ ). The effects of increasing the roughness length on clouds is not significant comparing to the effects of albedo and LAI.

If we only observe the evolution of cloud cover, Figure 9 gives a clearer picture of the effects of changing these values. Since the maximum cloud cover is around 25%, the figure confirms that the clouds from the online experiments are shallow cumulus clouds. Similar to Figure 8, the cloud cover from Figure 9.a indicates that the forest has more clouds than the grassland. This changes in cloud cover results from different values of albedo, roughness and LAI as is explained before.

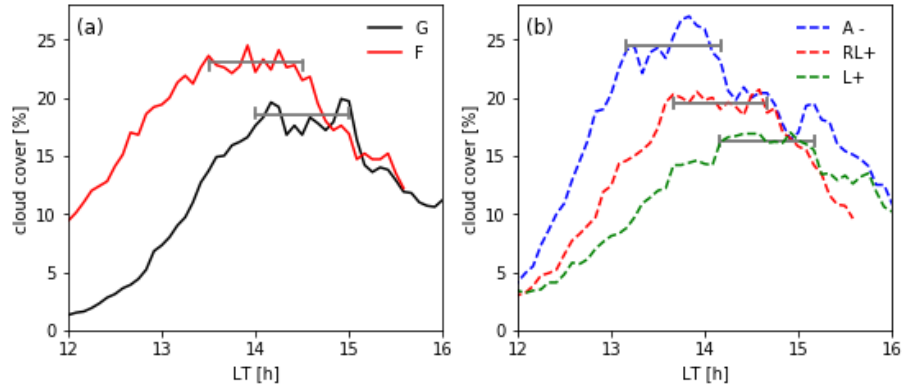


Figure 9: The cloud cover evolution from (a) the grassland (G, black solid line), forest (F, red solid line), Forest Albedo (A-, blue dashed line), roughness length + (RL+, red dashed line) and Forest LAI (L+, green dashed line). The grey whiskers represent the one-hour periods when the cloud cover reaches its maximum and stays rather constant and the periods are used in the following analysis (Figure 10).

Figure 9.b shows the effects of decreasing albedo, increasing roughness length and increasing the LAI separately in detail. Among all three, decreasing the albedo has the largest contribution to more clouds and its effect is more significant than the others. This is because in the Forest Albedo experiment, the overall absorption of incoming solar energy is around  $100 \text{ W m}^{-2}$  greater, whereas the two others (Forest Roughness Length and LAI) only change the partitioning of energy balance. With a greater net radiation, the skin temperature from this experiment is the highest (Figure 14), which may give rise to a faster increase of temperature than the air. Consequently, the surface sensible heat flux becomes larger. Because there is enough moisture provided in this study, the clouds are more sensitive to the sensible heat flux.

The individual effects of albedo, roughness length and LAI on cloud cover are similar to their effects on the sensible heat flux, whereas the combined effects follow the changes in the available energy. It means that overall effects of deforestation are dependent on the available energy (Figure 12 from the Appendix) and the clouds are very sensitive to the sensible heat flux variations.

### 3.3.2 Cloud layer energy release, inhibition and stability

Figure 10 reveals the data distribution of cloud cover and liquid water path from all five online experiments. From each experiment, a set of one-hour periods are collected and shown in Figure 9 when the cloud cover reaches its maximum and stays rather constant. The evaporative fraction is averaged over time for each experiment. Evaporative fraction (EF) is the fraction of latent heat flux

to the sum of sensible and latent heat fluxes

$$EF = \frac{LE}{H + LE}, \quad (2)$$

where EF is the evaporative fraction, the LE is the latent heat flux and the H is sensible heat flux. Evaporative fraction is used in this study because it is a useful diagnostic of the surface energy balance (Chen et al. 2018).

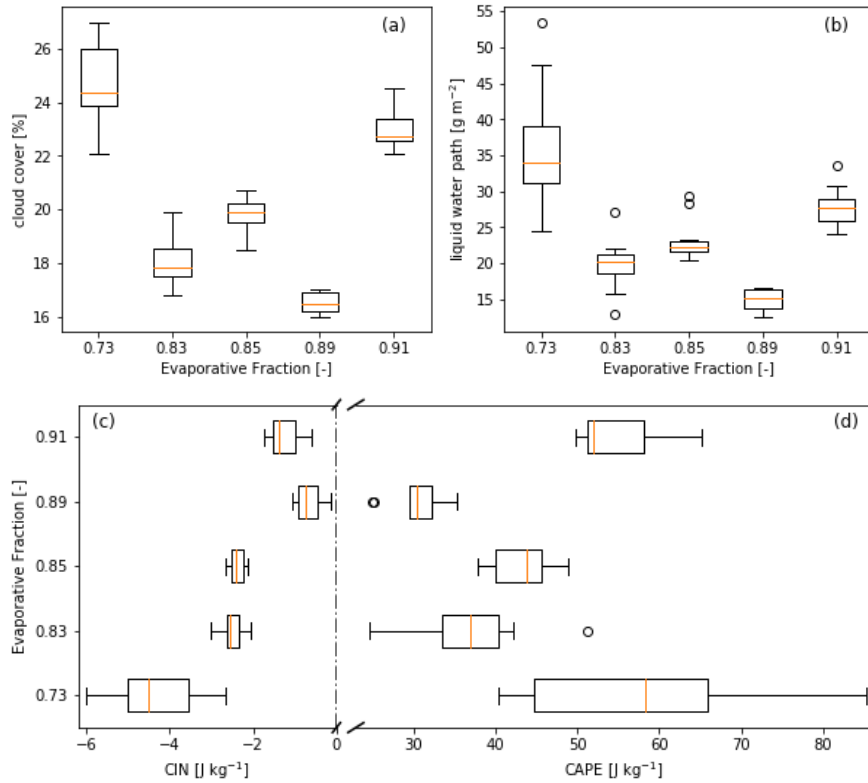


Figure 10: The box plots of (a) cloud cover, (b) liquid water path, (c) convective inhibition (CIN), and (d) convective available potential energy (CAPE) of different evaporative fractions (EF) from the one-hour periods defined in Figure 9 of all five online experiments). The upper and lower whiskers are the maximum and minimum values; the orange lines represent the medians; the box edges above and below the orange lines represent the interquartile ranges of the data selected; and the empty circles are the outliers that are out of the ranges set by 1.5 times the interquartile.

As can be seen from Figure 10, the cloud cover, liquid water path and CAPE have similar trends against the evaporative fraction, which means that the cloud cover and liquid water path are positively correlated. The relative magnitudes of the cloud cover and liquid water path in the selected one-hour periods are consistent to the previous results. Here, both CAPE and CIN are calculated from

the profiles of buoyancy flux. The CAPE is obtained by the positive area between zero and the buoyancy flux profiles above the entrainment zone and CIN is represented by the negative area indicating the entrainment zone.

As the changes in horizontal, vertical distributions of clouds, and the CAPE are consistent, it represents that a greater cloud cover and cloud liquid water are accompanied with the greater energy within the cloud layer. CIN on the other hand, shows an opposite trend comparing to the others. This is because it indicates the amount of energy that inhibits the turbulence, whereas the cloud cover, liquid water path and CAPE are positively affected by the turbulent energy. The greatest cloud cover and liquid water path are found in the Forest Albedo experiment. This experiment has the largest CAPE, however, it has the strongest CIN as well comparing to other experiments. As for the Forest LAI experiment, although it contains the smallest CAPE, it has the weakest CIN, and the overall effect of the two parameters gives rise to a smaller cloud cover. Therefore, Forest Albedo experiment has the greatest potential energy for developing the clouds among all the experiments and the Forest LAI has the least. Overall, from Figure 10, we can find an optimal condition when the evaporative fraction is equal to 0.73 as all the variables are optimised under this condition.

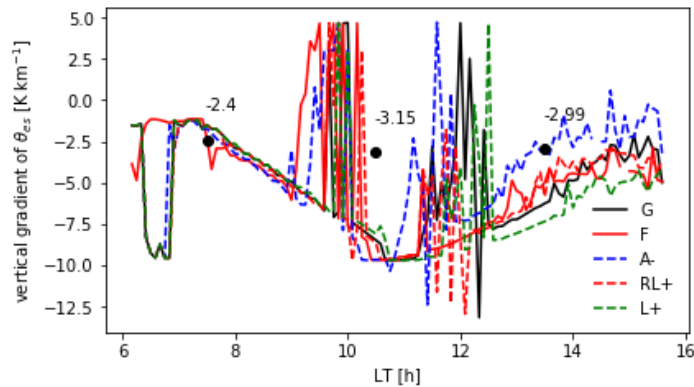


Figure 11: The temporal evolution of the vertical gradient of saturated equivalent potential temperature from the Grassland (G, solid black line), Forest (F, solid red line), Forest Albedo (A-, dashed blue line), Forest Roughness Length (RL+, dashed red line), Forest LAI (L+, dashed green line) and the observations (black dots, at 7:30, 10:30 and 13:30 LT).

In addition to the energy release and inhibition, the stability within the cloud layer also represents the states of the shallow cumulus clouds. Figure 11 shows the temporal evolution of the vertically averaged gradients of saturated equivalent potential temperature in the cloud layer from all five online experiments. The stability can be shown by the magnitudes of the vertical gradients and the greater values the more stable cloud layer (Bohren and Albrecht 2000) and the saturated equivalent

potential temperature is calculated by

$$\theta_{es} = \theta \exp\left(\frac{L_v w_s}{c_p T}\right), \quad (3)$$

where  $\theta$  is the potential temperature,  $L_v$  is the latent heat of vaporisation,  $w_s$  is the saturated mixing ratio,  $c_p$  is the specific heat of dry air, and  $T$  is temperature (Wallace and Hobbs 1977).

The values of the stability start from the same value due to the same initial potential temperature and specific humidity profiles. At 9:00 LT, evident differences can be seen. It is observable that before 9:00 LT, the stabilities change smoothly from all experiments and they start to fluctuate strongly until 12:30 LT when the cloud layers from the five experiments tend to become less unstable and decrease the range of fluctuations. The amplitudes of fluctuations of the stabilities from the Forest and Forest Albedo are significantly reduced earlier than the other three experiments. In contrast, a later and weaker stabilisation of cloud layers can be found from the Grassland, Forest Roughness Length, and Forest Albedo. Although, all fluctuations nearly disappear after 12:30 LT accompanied by an increasing of the stability, the values still indicate unstable cloud layers. As for the stability calculated from observations in the cloud layer, they are similar to the LES results. In the early morning (at 7:30 LT), the cloud layer is relatively less unstable than at 10:30 LT and 13:30 LT from the observations. Similar to the LES results, it is suggested a stabilisation of the cloud layer at 13:30 LT, by a slightly greater value of the gradient of  $\theta_{es}$  than at 10:30 LT.

Table 4: The one-hour averaged vertical gradient of saturated equivalent potential temperature ( $\gamma_{\theta_e}$ ) in the above the cloud layer, available energy (H+LE) from the surface, the CAPE and CIN

	<b>Grassland</b>	<b>Forest Albedo</b>	<b>Forest Roughness Length</b>	<b>Forest LAI</b>	<b>Forest</b>
$\gamma_{\theta_e}$ [K km <sup>-1</sup> ]	-3.72	-2.59	-3.79	-5.11	-4.58
H+LE [W m <sup>-2</sup> ]	453.67	606.34	520.00	446.67	654.78
CAPE [J kg <sup>-1</sup> ]	37.15	58.46	43.22	30.35	54.44
CIN [J kg <sup>-1</sup> ]	-2.51	-4.34	-2.39	-0.68	-1.25

\*The shaded cells show less stabilities from above and below the boundary layer than the Grassland

The stability has a negative relation with the evaporative fraction inter-experiments until it reaches the minimum value of -5.11 K km<sup>-1</sup> in the cloud layer with the evaporative fraction being 0.89 at the surface. When the evaporative fraction further increases to 0.91 (Forest), the latent heat flux is nine times greater than the sensible heat flux and this enhancement contributes to less instability in the cloud layer (Table 4).

Although the variations of them do not show any clear trend against evaporative fraction, they can

be explained by the stability within and above the top of the boundary layer (Table 4). In the table, the same one-hour periods are used for the averaged values. Both horizontal and vertical spread of the clouds are consistent to the available energy which is the sum of sensible and latent heat fluxes (H+LE) from the surface. The larger surface available energy, the greater cloud cover and liquid water path. A similar relation between CAPE and available energy can be found as well. Although CIN shows some variations, the magnitudes of the variations are much smaller than that of CAPE. It is worth noting that the lapse rate of the saturated equivalent potential temperature (gradient) has its smallest value in the Forest LAI and the largest in the Forest Albedo. The saturated equivalent potential temperature is the potential temperature with all the latent heat being released when the air is saturated. Smaller values of the  $\theta_{es}$  gradient stand for less stable atmosphere. Whereas with greater LAI, the cloud layer has the most unstable condition and decreasing the albedo counteracts the small effect of LAI. Thus, it can be concluded that the available energy and CAPE are dominant in the shallow cumulus clouds formation in this study.

Table 5: The components of one-hour averaged surface energy balance, surface temperature tendency, net radiation, velocity scales, and cloud properties

	<b>Grassland</b>	<b>Forest Albedo</b>	<b>Forest Roughness Length</b>	<b>Forest LAI</b>	<b>Forest</b>
EF [-]	0.83	0.73	0.85	0.89	0.91
H [ $\text{W m}^{-2}$ ]	74.32	153.13	76.10	48.74	58.42
LE [ $\text{W m}^{-2}$ ]	356.23	419.97	419.96	376.68	557.76
G [ $\text{W m}^{-2}$ ]	68.46	103.77	63.78	56.87	59.40
Rn [ $\text{W m}^{-2}$ ]	494.23	674.49	557.78	478.50	674.15
Ttend [ $\text{K h}^{-1}$ ]	-1.72	-0.86	-0.75	-1.368	-0.52
w* [ $\text{m s}^{-1}$ ]	1.48	1.89	1.49	1.27	1.41
u* [ $\text{m s}^{-1}$ ]	0.124	0.155	0.189	0.109	0.190
cloud cover [%]	18.08	24.77	19.78	16.49	22.98
cloud base [m]	1270	1413	1240	1075	1125
cloud top [m]	2748	2797	2770	2730	2777
LWP [ $\text{g m}^{-2}$ ]	19.85	36.13	23.15	14.93	27.72

Other variables that are also calculated from the several one-hour periods (defined in Figure 9) can be found from Table 5. They represent the surface sensible heat flux (H), latent heat flux (LE), ground heat flux (G), evaporative fraction (EF), net radiation (Rn), surface temperature tendency (Ttend), convective velocity scale (w\*), friction velocity (u\*), cloud liquid water path (LWP), cloud cover, base and top. As the pre-defined one hour periods are found when the cloud cover reaches the maximum and is rather constant, the values in Table 5 show the states of the shallow cumulus

cloud when it becomes stable.

Note that the decreases of net radiation inter-experiments can be seen from this table, although the cloud shading effect is not included here which makes this study less realistic. However, if it is included, the net radiation is expected to be even smaller than the current values in Table 5.

## 4 Discussion

In this section, our findings will be discussed and placed in context to the other studies. This section is organised by the following topics: spatial horizontal cloud distribution, cloud water content, energy release and inhibition, and the stability in the cloud layer stability. The variables related to the topics are cloud cover, liquid water path, CAPE, CIN and the vertical gradient of saturated equivalent potential temperature.

### 4.1 Cloud distribution

In the sensitivity analysis, the Forest Albedo experiment produces the most pronounced enhancement of cloud cover (15.1% maximum), followed by the Forest experiment (13.4%). Increasing the roughness length leads to similar results comparing to the Grassland (the enhancement is less than 6.3%) and a reduction of cloud cover is found in Forest LAI experiment (less than 3%). Among all sensitivity analyses, the Forest Albedo has the most significant changes in cloud cover whereas the Forest Roughness Length and LAI have the least. In this section, the percentages refer to the absolute changes of the shallow cumulus cloud cover.

In contrast to what we observe, other studies found that there was an enhancement of the shallow cumulus clouds over the deforested areas. Wen-Jian and Hai-Shan (2013) used the National Center of Atmospheric Research (NCAR) Community Atmospheric Model (CAM 4.0) and concluded that the land use or land cover change would enhance the cloud cover due to the changes in latent heat flux. This model has the resolution of  $1.9^\circ \times 2.5^\circ$  and mainly parameterises, whereas the LES used in this study is explicit and has the resolution of 53 m. The increase in cloud cover from their study is because the surface latent heat flux is increased and consequently the daily maximum temperature (Wen-Jian and Hai-Shan 2013). Additionally, Durieux, Machado, and Laurent (2003) discovered from the observations that the cumulus clouds tended to increase especially in the afternoon over the deforested area due to relatively stronger convection in this region. The deforestation from their study was accompanied by an increase of albedo. This is different from our study. As their shallow cumulus clouds were influenced by non-deforested areas, they considered the effects of the land heterogeneity and the resulted secondary circulation. Such heterogeneity effects were also studied by Wang, Bras, and Eltahir (2000), Wang et al. (2009) and Chagnon, Bras, and Wang (2004) from the observations that both the turbulence and the mesoscale circulations between the forest and the deforested regions contributed to the enhancement of cloud cover. A similar conclusion is also drawn by Heerwaarden and Vilà Guerau de Arellano (2008). They used the LES and found the surface heterogeneity may enhance cloud formation. However, note that the heterogeneity and mesoscale circulations are not included in our study because we have a homogeneous domain and

in the study we averaged the entire domain for the LES output. Therefore, the heterogeneity is not included in our research.

In opposition to the studies mentioned above, Dickinson and Kennedy (1992) found a reduction of cloud cover by using the NCAR CCM1 model with deforestation. However, according to Wang et al. (2009), deep clouds usually occur over the forest whereas the shallow cumulus clouds favour deforested areas. Therefore, the cloud cover reduction from the study of Dickinson and Kennedy (1992) is likely to be a result of the less deep clouds instead of shallow cumulus clouds. In our study, the overall shallow cumulus cloud cover is found to be less with deforestation (Grassland) and the reduction can be as large as 13.4%. Reasons for this could be that we used a different model and different observations as their parameterisation may result in incorrect findings whereas ours is explicitly resolved. Another reason is likely to be due to the lack of heterogeneity. As deforestation does not remove all the vegetation immediately, it is reasonable to consider a partly deforested area in this study. Additionally, the setup of the soil moisture from the model contributes to this result discrepancy as well. The initial soil moisture is kept at a relatively large value with the soil moisture index equal to 0.56. It provides the system with enough moisture supply and makes it a heat limited condition. Therefore, when more energy is partitioned to the sensible heat flux, the cloud cover increases significantly from the grassland, especially when the albedo decreases.

Regarding the surface friction, we find that our results are consistent to the study of Park, Böing, and Gentine (2018) which used the UCLA-LES and found a lower cloud cover with greater surface friction velocities. We also find an overall enhancement (less than 6.3%) of clouds when the roughness length is increased. Although the cloud cover shows a decrease of less than 2.3% after 15 LT, the difference between the Grassland control is small. This is partly because a very small wind speed is designed for the LES input ( $1 \text{ m s}^{-1}$ ) and it does not allow much impacts for increasing the roughness length on turbulence mixing. A study by Sikma et al. (2017) indeed found an increase of cloud cover with greater wind speeds. Furthermore, since our experiments only represent the canopy layer by the roughness length, the combination of a small wind speed and not including the canopy may give rise to the insensitive enhancement of cloud cover to the different roughness lengths.

Therefore, for future study, it is recommended to design a domain with partly deforested area and examine the effects of secondary circulations. Additionally, the effect of greater wind speeds (larger than at least  $5 \text{ m s}^{-1}$ ) and adding the canopy effects can be studied in order to find the intensified effects of increasing the roughness length. We also recommend to include the cloud shading effect to the experiments in order to obtain more realistic results.

## 4.2 Cloud liquid water

The liquid water path has similar results to the cloud cover from the sensitivity analysis. The Forest Albedo from our study has the greatest liquid water path (LWP) and the data distribution whereas the Forest LAI has the smallest LWPs. The Forest Albedo is followed by the Forest experiment and Forest Roughness Length has slightly greater liquid water path than the Grassland.

Overall, the results from our study are in line with the study of Nair et al. (2003). They used the Regional Atmospheric Modelling System to study the effects of the deforestation. Nair et al. (2003) found smaller domain average liquid water paths and smaller variabilities in the pasture than the forest. From our study, the reduction of LWP from Forest to Grassland is less than  $10 \text{ g m}^{-2}$ .

## 4.3 Energy release and inhibition in the cloud layer

The CAPE variations from the sensitivity analysis are closely related to the cloud cover and liquid water path. Generally, CAPE values need to be at least greater than  $400 \text{ J kg}^{-1}$  to trigger convective rainfall (Yin et al. 2015). However, the CAPE values from our study are always below  $100 \text{ J kg}^{-1}$ . For example, the maximum CAPE values from experiments Forest Albedo and Forest are 85 and  $65 \text{ J kg}^{-1}$ . The Forest LAI has the weakest CAPE among the five and a greater roughness triggers slightly greater CAPE values comparing to the Grassland. Overall, the CAPE values indicate small possibility for deep convection as the maximum values are less than  $100 \text{ J kg}^{-1}$ .

Firstly, our findings corroborate that forests usually have larger CAPEs than the deforested areas. Yin et al. (2015) found that the CAPE was large over the forest because of wetter soil, whereas their maximum soil moisture is  $0.45 \text{ m}^3 \text{ m}^{-3}$ . In our study, the initial soil moisture is kept at  $0.3 \text{ m}^3 \text{ m}^{-3}$  (soil moisture index at 0.56) and we find similar results as well. Wang et al. (2009) also found this relation and they had a savannah area within their study domain which was surrounded by the undisturbed forest. Then, the savannah generated the pre-discussed secondary circulations. Wang et al. (2009) argued that this area reacted more like a forest than a pasture and the forest had a greater humidity and a stronger CAPE, which might result in deeper clouds. The Forest experiment also generates wetter boundary layer and a stronger CAPE than the Grassland.

From the moisture perspective, enough supply of moisture from the surface also helps to increase CAPE values with low lifting condensation level (Yin et al. 2015). It is partly in line with our study that a wetter environment like Forest LAI and Forest have lower boundary layer heights than the Grassland (less than 200 m). Our results show that there is an optimal condition for the enhancement of shallow cumulus clouds regarding the energy partition and it occurs when the evaporative fraction is equal to 0.73. However, CAPE has smaller values in the Forest LAI than in

the Grassland, even though the latent sensible heat flux is relatively strong from Forest LAI. The strongest CAPE as observed in the Forest Albedo is indicated by a small inversion (less than 2°C).

A discrepancy is found from the study of Yin et al. (2015). They used several simplified zero-dimension mixed-layer models and concluded that the strongest deep convection occurred with the wettest soil when the entire temperature profiles were kept the same (Yin et al. 2015). However in our Forest LAI, a very wet surface is accompanied with the weakest CAPE with the values around 31 J kg<sup>-1</sup> with the evaporative fraction equal to 0.89. The strongest CAPE is found with the evaporative fraction equal to 0.73 (Forest Albedo). The only consistency occurs when comparing the Grassland and Forest which has a wetter boundary layer indicated by the specific humidity and a similar potential temperature profile. Their choice of the mixed-layer model could account for the differences between the studies, since it may not be good at focusing on the cloud layer.

Closely connected to CAPE, CIN stands for the cloud states as well, although it is the energy that the air parcels have to overcome before having further developments. Kalthoff et al. (2011) found from the observations that CIN had a negative relation to the convective boundary layer height because a lower boundary layer was capped by a strong inversion. From our research, CIN is weak in Forest LAI and has the values around -0.5 J kg<sup>-1</sup>. Whereas it is relatively strong in Forest Albedo at -4.5 J kg<sup>-1</sup>. The boundary layer heights are the lowest and the highest from two experiments respectively. Therefore there is a discrepancy as the effects of mountains included in their study whereas our study does not have any. Kalthoff et al. (2011) also discovered that CAPE and CIN did not always have positive correlation and this is similar to our findings as well.

Since the shallow cumulus clouds are sensitive to boundary layer conditions and hard to simulate, a large lapse rate is designed as above 2000 m for the initial input of LES. With this capping inversion, all clouds depth are controlled below two kilometers, but it does not have strong effects on the top of the cloud fraction. Because of the capping, no deep convection occurs in our study, even though the CIN values show as very weak. Future studies can focused on the effects of smaller potential temperature lapse rate while still in the context of shallow cumulus clouds and investigate the chances for deep convection.

#### **4.4 Stability in the cloud layer**

In this section, the atmospheric stability in the cloud layer is discussed because it shows the states of the cloud layer. It is defined by the vertical gradient of saturated equivalent potential temperature ( $\theta_{es}$ ). The stability in the cloud layer is shown in Table 4. From all experiments, the gradients of  $\theta_{es}$  are negative and ranges from -5.11 K km<sup>-1</sup> to -2.59 K km<sup>-1</sup> during the pre-defined one-hour

periods, representing conditionally unstable layers. In spite of similar initial conditions for all experiments, the Forest, Forest Roughness Length and Forest LAI, the cloud layers become more unstable than the Grassland, and the Forest LAI has the most unstable cloud layer. Interestingly, Forest Albedo has the least instability among all the five experiments given its strong CAPE.

What happens in the Forest Albedo can be explained by the droplet evaporation. As it has the greatest clouds and a very fast decrease of liquid water path (Figure 15) which inhibits the vertical mixing and stabilises the clouds (Albrecht 1989). Additionally, when the cloud base becomes too high, the evaporation below the cloud base forms a stable subcloud layer and makes the cloud and the subcloud layers decoupled (Albrecht 1989). In our study, the cloud base is highest from the Forest Albedo which is consistent to this theory.

Another reason to explain the stabilising of the cloud layer is related to the solar heating (Betts 1990) and radiative heating (Stevens and Feingold 2009). Betts (1990) claimed that with a rising cloud base, the sub-cloud layer warms and becomes more stable which may result in the decoupling of the cloud layer from the surface. This is in line with our study as a higher cloud base occurs in the Forest Albedo experiment. Furthermore, Stevens and Feingold (2009) used a global climate model and satellite data and claimed that the radiative heating was related to the stabilisation of the cloud layer when they studied the aerosol effects. The faster stabilisation of the cloud layer is accompanied by a faster increase of potential temperature but a faster decrease of temperature in the cloud layer in the Forest Albedo experiment (Figure 17). This is not consistent to the study of Stevens and Feingold (2009). However the cloud layer inversion slightly increases more in the Forest Albedo after 13:00 LT (see Figure 18) which indicates a stronger stabilisation in this layer. Therefore, this reason is less valid than the droplet evaporation in this study.

The stability in the cloud layer is also studied by Ek and Holtslag (2004) who used the observations and a one-dimensional (column) Coupled Atmospheric Boundary Layer Plant-Soil (CAPS) model to examine the effects of soil moisture on shallow cumulus clouds. They used the potential temperature lapse rate for the indication of stability. They found that with less stable and dry air above the atmosphere and with drier soil, more clouds were formed and the cloud cover was smaller for the greater stability and drier soil (Ek and Holtslag 2004). Our results are consistent with their study regarding the stability in the cloud layer, surface moisture content and cloud cover are combined. In our study, we found up to 13.4% more shallow cumulus clouds with less stability in the cloud layer and drier surface (less than  $2 \text{ g kg}^{-1}$ ). However, we also found a regime that the clouds were enhanced with more stability and wetter surface (less than  $1 \text{ g kg}^{-1}$ ). In indicating the trend of the stability, both their and our studies use the evaporative fraction. All our values of evaporative fractions are greater or equal than 0.73, which fall into the range of moister soil defined by Ek and

Holtslag (2004). Therefore, more energy is partitioned to latent heat flux than sensible heat flux from our study.

However, large values of evaporative fractions with respect to the study of Ek and Holtslag (2004) indicate enough moisture from the surface and instability from the cloud layer. Therefore, we suggest to design a new experiment with a smaller initial soil moisture index which brings the evaporative fraction to a lower value which indicates dry soil, but keep the other variables the same, and study their influences on the cloud evolution.

## 5 Conclusions

We investigated the land-atmosphere interactions during the dry season in the Amazon rainforest. To study this, we used a methodology that included the numerical experiments using the Dutch Atmospheric Large-Eddy Simulation (LES) that were constrained by the 30-day observations in September. The LES was used in order to find the effects of interactions and deforestation in the Amazon rainforest on shallow cumulus clouds formation.

We divided the research in parts with interconnected numerical experiments, therefore, three main experiments were conducted. The first two experiments were the control runs with an uncoupled surface (offline) and a coupled surface (online). The first two runs were controlled by surface conditions and the second experiment was characterised by a grassland. In order to achieve this, the variables, albedo, roughness length and LAI were set in the context of a grassland. The last experiment had the three variables changed from grassland to forest step by step and finally combined them in order to obtain a Forest scenario.

Our first aim was to validate the reliability of the LES and it was done by comparing the model results with the observations. Although some deviations occurred, the LES was validated well since the modelled results followed the observations. Secondly, we aimed to find the effects of including the interactions to the boundary layer by coupling a land surface model. When the LES was coupled with a land surface model, it showed a constrained boundary layer and a more passive cloud layer in the Amazon rainforest during the dry season. This was indicated by a shallower boundary layer, a less and later development of the shallow cumulus clouds after including the interactions. For example, the boundary layer was lowered less than 200 m, the shallow cumulus clouds started to develop around 20 min later and the cloud cover was approximately 2% less with the interactions. Other variables such as buoyancy flux demonstrated less active clouds as well with the buoyancy flux values  $0.01 - 0.02 \text{ K m s}^{-1}$  smaller than the offline experiment.

We took the coupled grassland experiment and systematically changed the albedo, roughness length and the LAI separately. In the last experiment, we combined the changes for all three variables. The overall effects showed a decline of cloud cover and the maximum of the decline was at 13.4%. The boundary layer was also less than 100 m deeper with deforestation and the liquid water path and cloud energy were reduced by the deforestation. The shallow cumulus clouds were found to be positively related to the available energy from the surface, especially when the energy was partitioned to the sensible heat flux.

In addition to the total effects of deforestation, the separate effects of the three parameters were examined. These experiments showed that the cloud was most sensitive to albedo and less sensitive

to roughness length and LAI. Therefore, decreasing the albedo resulted in the most evident enhancement of the cloud cover and the enhancement was as large as 15.1%. Whereas increasing the roughness length gave rise to less than 6.3% of cloud cover as well although there was around 2% less clouds after 15:00 LT comparing to the grassland scenario. It should be mentioned that the wind speed was designed very small which equaled to  $1 \text{ m s}^{-1}$ . Therefore, it suppressed the effects of increasing the roughness length which should have been more significant if with wind speeds greater than at least  $5 \text{ m s}^{-1}$ . When the LAI was increased, the our experiment showed a reduction of less than 3% of the cloud cover comparing to the grassland. It means that a greater leaf area counteracted the enhancement effects of albedo and roughness length for the shallow cumulus clouds.

Furthermore, the liquid water path and the CAPE were found to be greater in the all forest scenarios except for the Forest LAI which was smaller than the Grassland. The stability in the cloud layer defined by the vertical gradient of equivalent potential temperature also had a similar pattern inter experiments. The Forest Albedo had the least instability indicated by the vertical gradient of the saturated equivalent potential temperature ( $-2.59 \text{ K km}^{-1}$ ) and a faster rate to stabilisation. It was related to the cloud layer radiative heating and the decoupling from the subcloud layer due to a higher cloud base. Therefore, deforestation may lead to less shallow cumulus clouds, generally less energy release and cloud layer stability. The effects of each deforestation variable are different. They are stated as follows:

- decreasing the albedo enlarged the absorption of solar radiation (the maximum increase is  $97.8 \text{ W m}^{-2}$ ) and significantly enhanced the shallow cumulus cloud (15.1% maximum). As a result, it increased the cloud liquid water, the energy release but reduced the instability in the cloud layer in the period when the cloud cover reached the maximum and stabilised. In this experiment, it showed that the maximum cloud cover occurred with the evaporative fraction equal to 0.73 as an optimal condition;
- increasing the roughness length introduced more turbulence mixing and it gave rise to a small enhancement of shallow cumulus clouds (less than 6.3%) because of a small wind ( $1 \text{ m s}^{-1}$ ). It also enhanced the cloud liquid water, energy release and the instability;
- increasing the LAI enabled more energy to be partitioned to latent heat flux and suppressed the shallow cumulus cloud consequently. This change reduced the cloud liquid water, the energy release but increased the instability. Therefore, the thermals are more important than than the moisture content in this study.

In conclusion, our study mainly examined the effects of different surface conditions on shallow cumulus clouds formation because the whole system of clouds and surface was closely connected.

With the initial soil moisture index kept constant at 0.56, the entire study stayed within the regime where the moisture content was not a limiting factor from the surface. Surface energy, on the other hand, was partitioned to sensible and latent heat flux and it was demonstrated in the form of evaporative fraction and available energy. From the sensitivity analysis, we found that the shallow cumulus clouds were more easily formed if the boundary layer was characterised by a greater available energy with the forest. Additionally, an overall greater available energy made sure that the combined effects of moisture and heat created a favourable condition for the shallow cumulus cloud formation when observing the overall effect of deforestation. Apart from that, the surface energy partitioning is also essential because the maximum of shallow cumulus occurred when the evaporative fraction reached 0.73 when the albedo was changed to the forest. It was the condition when the thermals had their greatest influences on the energy balance from this study. As a stronger thermal was able to bring the moisture from surface to the upper air, more shallow cumulus clouds could be formed.

Depending on our study, future studies are recommended to focus on a drier soil as the initial set of the soil moisture in this study is very large and constant. It is also recommended to introduce the land surface heterogeneity in order to study the effects of secondary circulations with LES. Another experiment can also be conducted with a larger wind speed so that the effects of roughness length is enlarged and more observable. Additionally, the potential temperature lapse rate can be made smaller at higher level to remove the effects of strong capping. Lastly, it is highly recommended to include the cloud shading effect to the LES as it helps simulate a more realistic boundary layer.

## **Acknowledgements**

I would like to express my gratitude to my supervisor Jordi Vilà-Guerau de Arellano who always tried to devote more time to guiding and helping me whenever I needed it. He was also consistently patient to give me precious advice when I had questions.

All the observations used to reproduce the plots and tables were obtained from the GOAmazon campaign and I would like to thank them for it. Thanks to Pierre Gentine who provided all these data for our study. I would also like to thank Ingrid van der Laan-Luijkx for giving me the data and advice on how to quantify the effects of forest fires in this study.

I give my thanks to Chiel van Heerwaarden who provided me with a paper and inspired new ideas for designing the experiments. Thanks again to Chiel van Heerwaarden, Xabier Pedruzo-Bagazgoitia and Yang Liu for their help on the Python codes at the beginning and the final stages of the thesis. I would like to thank Kees van den Dries and Erik van Schaik Kees for installing the softwares and coding packages on my computer and laptop.

Furthermore, I am grateful to have all my peers from the thesis ring as they provided me with a lot of very useful feedbacks on my submissions. Lastly, many thanks to my friends and family for their support and company all the way.

## References

- Albrecht, Bruce A. 1989. “Aerosols, cloud microphysics, and fractional cloudiness”. *Science* 245 (4923): 1227–1230.
- Anber, Usama, Pierre Gentine, Shuguang Wang, and Adam H Sobel. 2015. “Fog and rain in the Amazon”. *Proceedings of the National Academy of Sciences* 112 (37): 11473–11477.
- Avissar, Roni, Patricia Avissar, Ytzhag Mahrer, and Ben Ami Bravdo. 1985. “A model to simulate response of plant stomata to environmental conditions”. *Agricultural and Forest Meteorology* 34 (1): 21–29.
- Beltrán-Przekurat, Adriana, Roger A Pielke Sr, Joseph L Eastman, and Michael B Coughenour. 2012. “Modelling the effects of land-use/land-cover changes on the near-surface atmosphere in southern South America”. *International Journal of Climatology* 32 (8): 1206–1225.
- Betts, Alan K. 1990. “Diurnal variation of California coastal stratocumulus from two days of boundary layer soundings”. *Tellus A: Dynamic Meteorology and Oceanography* 42 (2): 302–304.
- Bohren, Craig F, and Bruce A Albrecht. 2000. *Atmospheric thermodynamics*.
- Chagnon, FJF, RL Bras, and J Wang. 2004. “Climatic shift in patterns of shallow clouds over the Amazon”. *Geophysical Research Letters* 31 (24).
- Chen, Liang, Paul A Dirmeyer, Zhichang Guo, and Natalie M Schultz. 2018. “Pairing FLUXNET sites to validate model representations of land-use/land-cover change”. *Hydrology and Earth System Sciences* 22 (1): 111.
- Collow, Allison B Marquardt, Mark A Miller, and Lynne C Trabachino. 2016. “Cloudiness over the Amazon rainforest: Meteorology and thermodynamics”. *Journal of Geophysical Research: Atmospheres* 121 (13): 7990–8005.
- Dickinson, Robert E, and Patrick Kennedy. 1992. “Impacts on regional climate of Amazon deforestation”. *Geophysical Research Letters* 19 (19): 1947–1950.
- Durieux, Laurent, Luiz Augusto Toledo Machado, and Henri Laurent. 2003. “The impact of deforestation on cloud cover over the Amazon arc of deforestation”. *Remote Sensing of Environment* 86 (1): 132–140.
- Ek, MB, and AAM Holtslag. 2004. “Influence of soil moisture on boundary layer cloud development”. *Journal of hydrometeorology* 5 (1): 86–99.
- Heerwaarden, Chiel C van, and Jordi Vilà Guerau de Arellano. 2008. “Relative humidity as an indicator for cloud formation over heterogeneous land surfaces”. *Journal of the Atmospheric Sciences* 65 (10): 3263–3277.

- Heus, Thijs, et al. 2010. “Formulation of the Dutch Atmospheric Large-Eddy Simulation (DALES) and overview of its applications”. *Geoscientific Model Development* 3 (2): 415.
- Hilker, Thomas, et al. 2015. “On the measurability of change in Amazon vegetation from MODIS”. *Remote Sensing of Environment* 166:233–242.
- Horn, GL, HG Ouwensloot, J Vilà-Guerau De Arellano, and M Sikma. 2015. “Cloud shading effects on characteristic boundary-layer length scales”. *Boundary-Layer Meteorology* 157 (2): 237–263.
- Kalthoff, N, et al. 2011. “The dependence of convection-related parameters on surface and boundary-layer conditions over complex terrain”. *Quarterly Journal of the Royal Meteorological Society* 137 (S1): 70–80.
- Khanna, Jaya, and David Medvigy. 2014. “Strong control of surface roughness variations on the simulated dry season regional atmospheric response to contemporary deforestation in Rondônia, Brazil”. *Journal of Geophysical Research: Atmospheres* 119 (23).
- Martin, Scot T, et al. 2017. “The green ocean Amazon experiment (GoAmazon2014/5) observes pollution affecting gases, aerosols, clouds, and rainfall over the rain forest”. *Bulletin of the American Meteorological Society* 98 (5): 981–997.
- Nair, Udaysankar S, Robert O Lawton, Ronald M Welch, and Roger A Pielke. 2003. “Impact of land use on Costa Rican tropical montane cloud forests: Sensitivity of cumulus cloud field characteristics to lowland deforestation”. *Journal of Geophysical Research: Atmospheres* 108 (D7).
- Park, Seung-Bu, Steven Böing, and Pierre Gentine. 2018. “Role of Surface Friction on Shallow Nonprecipitating Convection”. *Journal of the Atmospheric Sciences* 75 (1): 163–178.
- Phillips, Oliver L, et al. 2009. “Drought sensitivity of the Amazon rainforest”. *Science* 323 (5919): 1344–1347.
- Quesada, Benjamin, Almut Arneth, and Nathalie Noblet-Ducoudré. 2017. “Atmospheric, radiative, and hydrologic effects of future land use and land cover changes: A global and multimodel climate picture”. *Journal of Geophysical Research: Atmospheres* 122 (10): 5113–5131.
- Saatchi, Sasan S, Joao Viane Soares, and Diogenes Salas Alves. 1997. “Mapping deforestation and land use in Amazon rainforest by using SIR-C imagery”. *Remote Sensing of Environment* 59 (2): 191–202.
- Siebesma, A Pier, et al. 2003. “A large eddy simulation intercomparison study of shallow cumulus convection”. *Journal of the Atmospheric Sciences* 60 (10): 1201–1219.

- Sikma, M, HG Ouwersloot, X Pedruzo-Bagazgoitia, CC van Heerwaarden, and J Vilà-Guerau de Arellano. 2017. “Interactions between vegetation, atmospheric turbulence and clouds under a wide range of background wind conditions”. *Agricultural and Forest Meteorology*.
- Stevens, Bjorn, and Graham Feingold. 2009. “Untangling aerosol effects on clouds and precipitation in a buffered system”. *Nature* 461 (7264): 607.
- Vilà-Guerau de Arellano, Jordi, Huug G Ouwersloot, Dennis Baldocchi, and Cor MJ Jacobs. 2014. “Shallow cumulus rooted in photosynthesis”. *Geophysical Research Letters* 41 (5): 1796–1802.
- Vilà-Guerau de Arellano, Jordi, Edward G Patton, Thomas Karl, Kees van den Dries, Mary C Barth, and John J Orlando. 2011. “The role of boundary layer dynamics on the diurnal evolution of isoprene and the hydroxyl radical over tropical forests”. *Journal of Geophysical Research: Atmospheres* 116 (D7).
- Wallace, JM, and PV Hobbs. 1977. “Atmosphere science-an introductory survey.” *Atmospheric Science*: 468.
- Wang, Jingfeng, Rafael L Bras, and Elfatih AB Eltahir. 2000. “The impact of observed deforestation on the mesoscale distribution of rainfall and clouds in Amazonia”. *Journal of Hydrometeorology* 1 (3): 267–286.
- Wang, Jingfeng, et al. 2009. “Impact of deforestation in the Amazon basin on cloud climatology”. *Proceedings of the National Academy of Sciences* 106 (10): 3670–3674.
- Wen-Jian, Hua, and Chen Hai-Shan. 2013. “Impacts of regional-scale land use/land cover change on diurnal temperature range”. *Advances in climate change research* 4 (3): 166–172.
- Yin, Jun, John D Albertson, James R Rigby, and Amilcare Porporato. 2015. “Land and atmospheric controls on initiation and intensity of moist convection: CAPE dynamics and LCL crossings”. *Water Resources Research* 51 (10): 8476–8493.

## A Supporting figures for the sensitivity analysis

In this section, the figures used for supporting the sensitivity analysis are showed. The most relevant figures have been put to the main text whereas, they are not completely valid without these figures. Figure 12, 13, and 14 indicate the most basic surface energy partitioning, net radiation and temperature changes for all five online experiments, whereas Figure 15 and 16 complete the information which Figure 8 and 10 did not demonstrate. On the other hand, Figure 17 and 18 show the cloud layer temperature and inversion from all online experiments.

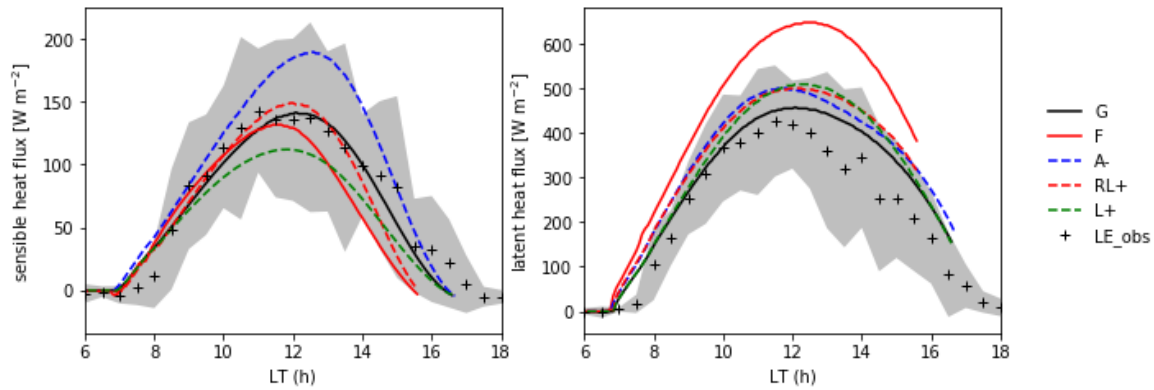


Figure 12: The temporal evolutions of the sensible (a) and latent heat flux (b) from the Grassland (G, solid black line), Forest (F, solid red line), Forest Albedo (A-, dashed blue line), Forest Roughness Length (RL+, dashed red line), Forest LAI (L+, dashed green line) and the averaged 30-day observations (black crossings). The shaded areas are the ranges of standard deviations.

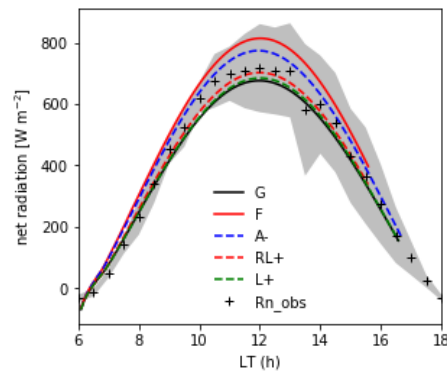


Figure 13: The temporal evolution of net radiation from the Grassland (G, solid black line), Forest (F, solid red line), Forest Albedo (A-, dashed blue line), Forest Roughness Length (RL+, dashed red line), Forest LAI (L+, dashed green line) and the averaged 30-day observations (black crossings). The shaded area is the range of standard deviations.

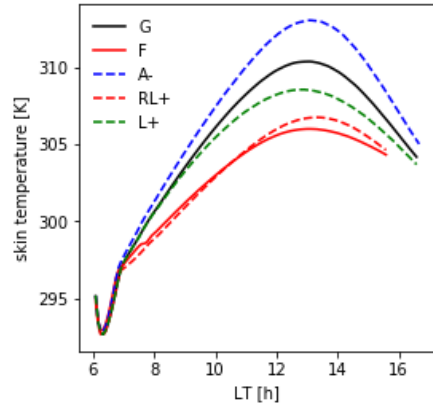


Figure 14: Time evolution of skin temperature from the Grassland (G, solid black line), Forest (F, solid red line), Forest Albedo (A-, dashed blue line), Forest Roughness Length (RL+, dashed red line) and Forest LAI (L+, dashed green line).

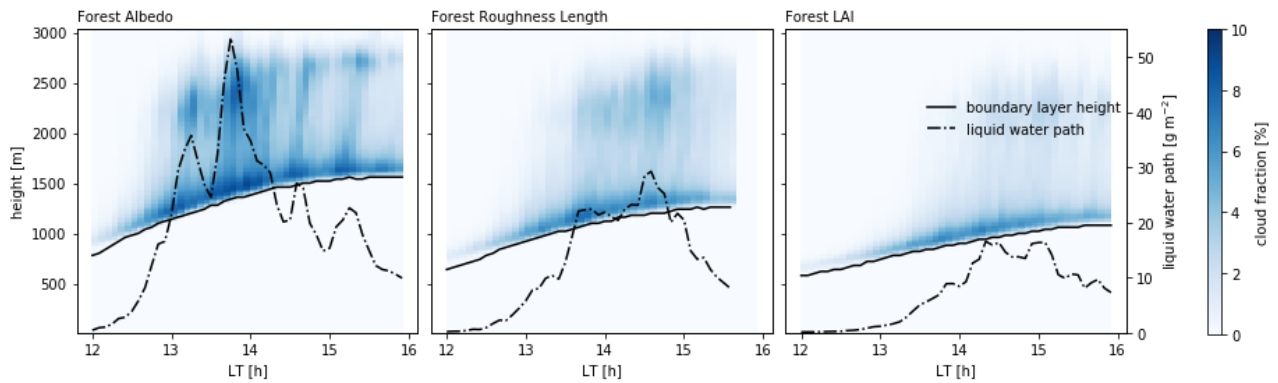


Figure 15: Temporal evolutions of cloud fraction (colour band), boundary layer height (black solid lines), and the liquid water path (black dashed lines) of the Forest Albedo (left), Forest Roughness Length (middle) and the Forest LAI (right) experiments.

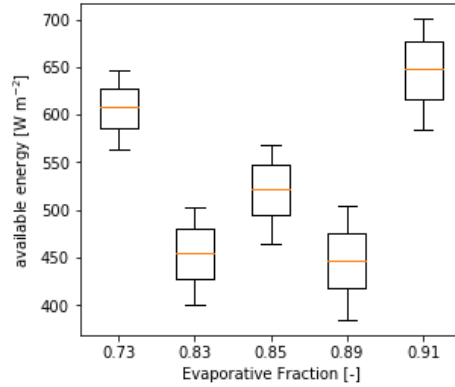
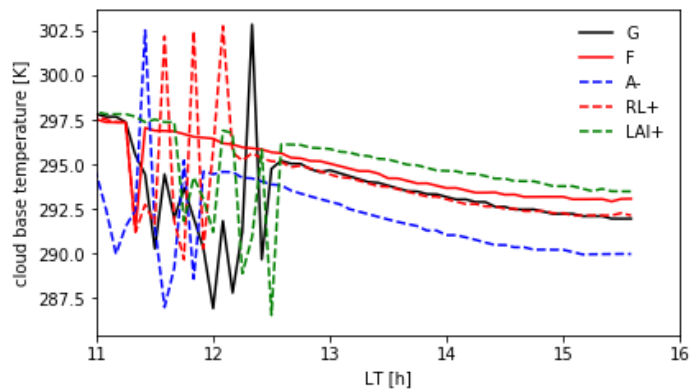
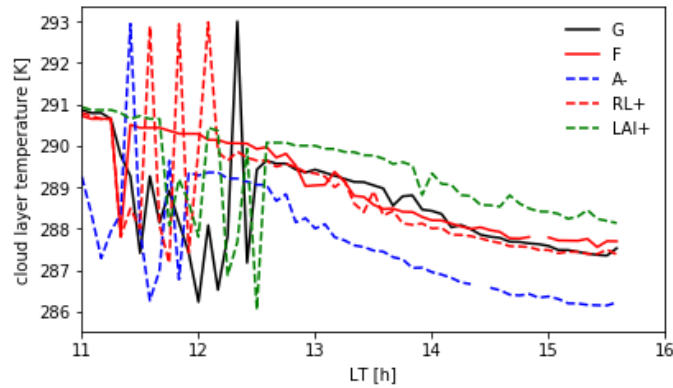


Figure 16: The box plot of available energy of different evaporative fractions (EF) from the one-hour periods defined in Figure 9 of all five online experiments). The upper and lower whiskers are the maximum and minimum values; the orange lines represent the medians; the box edges above and below the orange lines represent the interquartile ranges of the data selected; and the empty circles are the outliers that are out of the ranges set by 1.5 times the interquartiles.



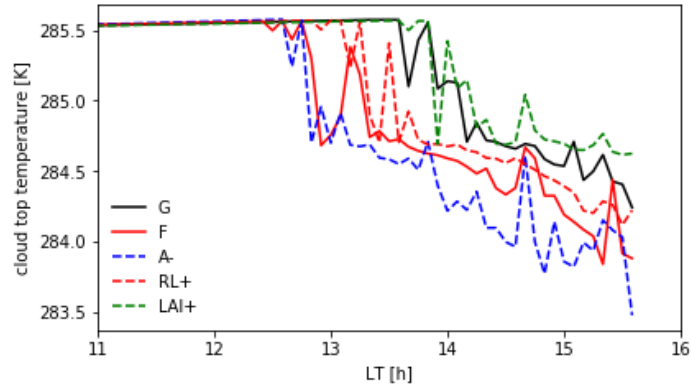


Figure 17: Time evolutions of cloud layer average temperature (top), cloud base temperature (middle) and cloud top temperature (bottom) from the Grassland (G, solid black line), Forest (F, solid red line), Forest Albedo (A-, dashed blue line), Forest Roughness Length (RL+, dashed red line) and Forest LAI (L+, dashed green line).

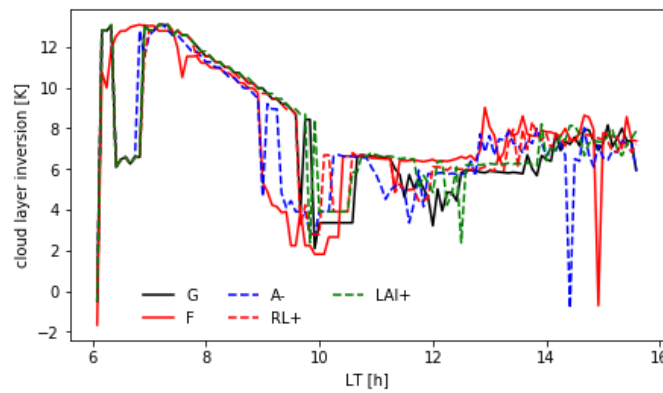


Figure 18: Time evolution of cloud layer inversions from the Grassland (G, solid black line), Forest (F, solid red line), Forest Albedo (A-, dashed blue line), Forest Roughness Length (RL+, dashed red line) and Forest LAI (L+, dashed green line).